https://doi.org/10.5194/egusphere-2026-2942
Preprint. Discussion started: 17 July 2026

The Regional Oceanic Modeling System with Non-Conservative Surface Gravity Wave Effects on Currents (ROMS-NCWEC v1.0.0)

Delphine Hypolite[1], Daniel P. Dauhajre[2], Minna Ho[1], Leonel Romero[3], and James C. McWilliams[1]

[1]Department of Atmospheric and Oceanic Sciences, University of California, Los Angeles, Los Angeles, California.
[2]Department of Geography, University of California, Santa Barbara, Santa Barbara, California.
[3]Department of Marine Sciences, University of Connecticut, Groton, Connecticut.

Correspondence: Delphine Hypolite (dhypolite@atmos.ucla.edu)

Abstract. We present ROMS-NCWEC, an updated and extended implementation of non-conservative Wave Effects on Currents (WEC) in the Regional Ocean Modeling System (ROMS). It is either one-way coupled to the spectral wave model WaveWatch3 (WW3) to resolve a broadband wave field or fully coupled to a spectrum-peak (WKB) wave model with Doppler-shift Current Effects on the waves (CEW). The implementation of three non-conservative (NC) effects includes the following: wave breaking and wave-induced bottom streaming, each represented as either a boundary stress or a 3D body force, and wave-enhanced bottom drag. The turbulent mixing from wave breaking is parameterized as a near-surface eddy viscosity enhancement to the K-Profile Parameterization (KPP) model. The bottom boundary layer mixing scheme is modified to account for the influence of wave streaming and wave-enhanced bottom drag. The implementation is validated against the Duck 1994 experiment, recovering the essential nearshore flow features with normalized RMS errors comparable to past studies. ROMS-NCWEC is then applied in a realistic regional setting near Pt. Arguello, CA. It uses an intermediate grid resolution ($dx = 30$ m) that is inner-shelf-resolving, surfzone-permitting that bridges the gap between coarse-grid regional models and more fully surfzone-resolving simulations. A momentum balance analysis reveals dynamically distinct offshore and nearshore regimes. Offshore, WEC amplifies the terms in the turbulent thermal wind balance while preserving it as the governing balance, consistent with prior findings on wave-enhanced frontogenesis. Nearshore, breaking stress emerges as the dominant WEC contribution, producing at times vorticity enhancements of order 20 times relative to a no-wave control case and shifting the balance from wind-versus-drag to breaking-plus-wind-versus-drag. Wave streaming is found to compete with bottom drag on the inner shelf (depths $10\,\mathrm{m} < h < 100\,\mathrm{m}$). Just seaward of the breaking zone, streaming meets the wave-driven undertow return current; the resulting near-bed convergence drives upwelling that closes a wave-forced overturning cell and generates strongly sheared alongshore jets at the surface.

1 Introduction

Wave effects on currents (WEC) is a fundamental component of coastal oceanic dynamics. Near the surface, breaking waves inject momentum, enhance turbulent mixing, and drive nearshore circulation. Near the bottom, wave orbital motions amplify bed friction and generate a streaming acceleration in the direction of wave propagation. These non-conservative processes

https://doi.org/10.5194/egusphere-2026-2942
Preprint. Discussion started: 17 July 2026

shape the momentum balance across the inner shelf and surfzone, influencing currents, cross-shelf exchange, and coastal tracer transport (Lentz et al., 1999; Lentz and Fewings, 2012; Feddersen and Trowbridge, 2005; Wang et al., 2020).

At the regional scale, waves interact with submesoscale currents, fronts, and vortices in the range O(100m–1km) with Rossby number of order one or larger. This is now recognized as dynamically important for vertical exchange (McWilliams, 2016) and coastal connectivity (Dauhajre et al., 2017, 2019). Wave effects, through the vortex force, can intensify submesoscale fronts and cyclonic vorticity (Hypolite et al., 2021), motivating their inclusion in regional ocean models.

Prior WEC implementations in realistic settings fall into two methodological families. Phase-resolving models, including 2D depth-averaged Boussinesq models, such as FUNWAVE (Kirby et al., 1998; Shi et al., 2012), and 3D non-hydrostatic models such as SWASH (Zijlema et al., 2011) and CROCO (Treillou et al., 2025), explicitly resolve individual wave phases and surfzone vorticity generation, but at computational costs that restrict domains to O(100m–1km) in cross-shore extent, precluding representation of regional circulation and submesoscale dynamics. Phase-averaged models, in which wave effects on currents are represented through a wave-averaged framework, span a broader range of scales. Surfzone-resolving phase-averaged models achieve fine resolution in the breaking zone, explicitly representing nearshore circulation including undertow, rip currents, and setup gradients, and either operate in idealized domains (e.g. Uchiyama et al., 2010; Wang et al., 2020) or employ telescoping grids in which the regional domain feeding the nearshore remains coarse, with horizontal diffusion required for stability at the grid transition (e.g. Kumar et al., 2012). Using such a telescoping configuration, Wu et al. (2021) showed that surfzone wave effects propagate significantly onto the inner shelf, substantially altering flow variability and tracer transport, highlighting the importance of the nearshore-inner-shelf regime for regional circulation. These implementations also typically rely on spectrum-peak wave forcing, which has been shown to systematically underestimate Stokes drifts in mixed wind-sea and swell conditions (Kumar et al., 2017; Romero et al., 2021). By contrast, regional ocean models operating at O(100m–1km) horizontal grid resolution capture the broader coastal circulation (Hypolite et al., 2021) but leave the surfzone unresolved. The intermediate regime has remained unexplored: a realistic regional domain at uniform O(10–100m) resolution that resolves the inner shelf, the dynamical bridge between surfzone and shelf circulation, retaining regional mesoscale and submesoscale currents. This regime opens access to inner-shelf processes including internal wave shoaling, tidal bore propagation, and wave-modulated cross-shelf exchange, which depend on resolving the inner shelf within its regional context. Here we present ROMS-NCWEC, an updated implementation of non-conservative WEC in ROMS one-way coupled to WW3, applied for the first time in a realistic regional setting at $dx = 30$m uniform grid resolution without any added horizontal diffusion and with broadband wave forcing.

Shchepetkin and McWilliams (2003, 2005) ROMS is a generalized terrain-following-coordinate, split-explicit, free-surface oceanic circulation model solving the primitive equations under hydrostatic or non-hydrostatic balance (Roullet et al., 2017). It uses the Boussinesq approximation with a realistic equation of state for seawater and physical parameterizations of the top and bottom boundary layers (KPP; Large et al., 1994). Its pressure-gradient, advection, and time-stepping algorithms are designed for robust accuracy in highly turbulent flows, ensuring exact finite-volume conservation and limiting numerical diffusion of tracer properties. Surface turbulent fluxes are estimated using bulk formulae including a current feedback on surface wind stress (Renault et al., 2016).

https://doi.org/10.5194/egusphere-2026-2942
Preprint. Discussion started: 17 July 2026

WEC was first implemented in ROMS by Uchiyama et al. (2010) (hereafter U2010) using the asymptotic wave-averaged, quasi-linear framework of McWilliams et al. (2004), which exploits the time-scale separation between short-period waves and longer-period currents to represent wave effects without resolving individual wave phases, assuming wind-wave equilibrium and small wave slope. This framework adopts the vortex force formalism, which has been shown to correctly represent 3D wave-mean flow interaction in ways that radiation stress formulations cannot (Ardhuin et al., 2008; Lane et al., 2007; Ardhuin et al., 2017), encompassing conservative effects including the Stokes-Coriolis force, Stokes shear force, Bernoulli head, and quasi-static set-down, alongside non-conservative effects including wave breaking, bottom streaming, and enhanced bottom drag. U2010 demonstrated ROMS-NCWEC capabilities in idealized settings including the Duck 1994 benchmark and plane beach configurations. Here we present an updated and extended implementation of ROMS-NCWEC consistent with the current UCLA codebase, incorporating the broadband formulation of Romero et al. (2021) through one-way coupling with the Wave Height, Water Depth, and Current Hindcasting third generation wave model (WaveWatch3, WW3; Tolman, 2009), validated against the same Duck94 benchmark for continuity with U2010, and applied for the first time in a realistic coastal regional setting at $dx = 30$m uniform resolution without horizontal diffusion.

All operational spectral wave models in variable environments rest on a WKB framework with an assumed scale separation between the primary waves and the slowly varying environment. Third-generation models such as WW3 and SWAN (Booij et al., 1999) supplement this framework with parameterized source and sink terms representing wind input, dissipation, and nonlinear cross-wavenumber transfers. The reduced wave description used here adopts the same WKB foundation with a more limited treatment of the source-sink physics.

Beyond the codebase update, this implementation extends the non-conservative WEC framework of U2010 in several directions. We introduce a modified bottom boundary layer thickness criterion accounting for wave streaming, and improve the temporal consistency of WEC forces and KPP mixing by recomputing both at the corrector stage of the predictor-corrector time stepping scheme.

The paper is organized as follows. Section 2 describes the governing equations of the wave-averaged framework. Section 3 recalls conservative WEC expressions including the spectrum-peak and broadband Stokes drift, Bernoulli head, set-down and pressure correction while indicating the required variables of the one-way coupling with WW3. Section 4 details the three non-conservative wave effects: wave breaking, wave-induced bottom streaming, and wave-enhanced bottom drag. Section 5 reproduces the Duck 1994 experiment as a benchmark validation of the updated implementation. Section 6 presents a regional application illustrating the dynamical implications of non-conservative WEC in a surfzone-permitting realistic setting, including the momentum balance structure that emerges in this new intermediate regime. Section 7 provides a summary and discussion. Appendix A provides the compilation option tree as a practical reference for users implementing ROMS-NCWEC. Appendix B recalls the equations of the WKB solver, available in ROMS-NCWEC as an alternative to WW3 forcing. Appendix C provides a list of symbol definitions.

https://doi.org/10.5194/egusphere-2026-2942
Preprint. Discussion started: 17 July 2026

2 Governing equations

We recall here how WEC modifies the Primitive Equations in the quasi-linear, vortex-force formalism U2010. In Cartesian coordinates (x, y, z), the momentum equation with WEC is

$$\partial_t \mathbf{u} + (\mathbf{u} \cdot \nabla_\perp)\mathbf{u} + w\partial_z \mathbf{u} + f\hat{\mathbf{z}} \wedge \mathbf{u} + \nabla_\perp \phi - \mathbf{F} = -\nabla_\perp \mathscr{K} + \mathbf{J} + \mathbf{F}^{\mathrm{w}} \,. \tag{1}$$

Boldface symbols are vectors in the horizontal plane (x, y), and the subscript $\perp$ further indicates a horizontal derivative. The generalized hydrostatic balance equation is

$$\partial_z \phi + \frac{g\rho}{\rho_0} = -\partial_z \mathscr{K} + K \,. \tag{2}$$

The incompressible mass conservation equation is

$$\nabla_\perp \cdot \mathbf{u} + \partial_z w = 0 \,. \tag{3}$$

The Eulerian 3D velocity field is $(\mathbf{u}, w)$, and the geopotential function ϕ is pressure normalized by a reference density ρ_0. The gravitational constant is g. The usual Non-Conservative (NC) forces in ROMS are represented by $\mathbf{F}$, including the parameterized vertical mixing and an implicit hyperdiffusion term, [1]

$$\mathbf{F} = \frac{\partial}{\partial z}(K_v \mathbf{u}_z) + \mathcal{D}_\perp \,, \tag{4}$$

with K_v is the turbulent eddy viscosity. With a superscript w, $\mathbf{F}^{\mathrm{w}}$ denotes non-conservative forces induced specifically by surface gravity waves (Sec. 4).

The equation for tracers c (like temperature and salinity) is

$$\partial_t c + (\mathbf{u} \cdot \nabla_\perp)c + w\partial_z c - \mathscr{C} = -(\mathbf{u}^{\mathrm{St}} \cdot \nabla_\perp)c - w^{\mathrm{St}}\partial_z c \,, \tag{5}$$

with $\mathscr{C}$ the non-conservative tracer forcing including surface/bottom fluxes plus the turbulent diffusion $\partial_z(K_t \partial_z c)$ supplied by KPP[2]. The set of Eq. (1), (2), (3) and (5) are completed by the equation of state from Jackett and Mcdougall (1995).

At the surface, the pressure continuity condition is

$$g\eta^c - \phi^c|_{\eta^c} = \mathscr{P} + g\hat{\eta} - \mathscr{K}|_{\eta^c} \,, \tag{6}$$

where $\eta^c = \eta + \hat{\eta}$, $\phi^c = \phi + \mathscr{K}$, and $\mathscr{P}$ is a pressure correction term.

The boundary condition

$$w|_{-h} + \mathbf{u}|_{-h} \cdot \nabla_\perp h = 0 \,, \tag{7}$$

[1] $\mathcal{D}_\perp$ represents implicit numerical diffusion arising from the upstream-biased advection scheme of ROMS (Shchepetkin and McWilliams, 2005).

[2] The WEC modified tracer equation used to contain an extra wave-induced tracer diffusivity $\mathscr{E}$ which was dropped for realistic application because it represents reversible wave-orbital kinematic spreading and its time-derivative form (Eq. 6 in U2010) goes negative whenever the wave amplitude envelope decreases, producing unphysical anti-diffusion in the implicit tracer solver.

https://doi.org/10.5194/egusphere-2026-2942
Preprint. Discussion started: 17 July 2026

ensures no-flux through the bottom (flow-tangency) and

$$w|_{\eta+\hat{\eta}} - \partial_t \eta - (\mathbf{u}|_{\eta+\hat{\eta}} \cdot \nabla_\perp)\eta = \mathbf{U}^{\mathrm{St}} + \partial_t \hat{\eta} + (\mathbf{u}|_{\eta+\hat{\eta}} \cdot \nabla_\perp)\hat{\eta}\,, \tag{8}$$

is the kinematic free-surface condition that makes the Stokes drift transport divergence ($\nabla_\perp \mathbf{U}^{\mathrm{St}}$) the effective surface flux of the Eulerian-mean flow, with the Stokes drift transport defined as

$$\mathbf{U}^{\mathrm{St}} = \int_{-h}^{\eta+\hat{\eta}} \mathbf{u}^{\mathrm{St}} dz\,. \tag{9}$$

3 Conservative wave effects on currents

In the momentum equations (1)-(2), the conservative WEC terms are the horizontal vortex force $\mathbf{J}$,

$$\mathbf{J} = -\hat{\mathbf{z}} \wedge \mathbf{u}^{\mathrm{St}}\left((\hat{\mathbf{z}} \cdot \nabla_\perp \wedge \mathbf{u}) + f\right) - w^{\mathrm{St}} \partial_z \mathbf{u}\,, \tag{10}$$

the vertical vortex force K,

$$K = \mathbf{u}^{\mathrm{St}} \cdot \partial_z \mathbf{u}\,, \tag{11}$$

the Bernoulli head $\mathscr{K}$, and the quasi-static set-down $\hat{\eta}$ which adds up to the sea surface height and comes into play in the surface boundary condition (6).

To evaluate these forces, the horizontal Stokes drift $\mathbf{u}^{\mathrm{St}}$, Bernoulli head $\mathscr{K}$, quasi-static set-down $\hat{\eta}$ and $\mathscr{P}$ need to be expressed with wave input variables. The expression for the vertical component of the Stokes drift w^{St} is not required as it is obtained from the incompressible continuity equation for the 3D Stokes drift,

$$\nabla_\perp \cdot \mathbf{u}^{St} + \partial_z w^{St} = 0\,. \tag{12}$$

These conservative WEC terms are expressed from knowledge of the wave field, i.e., the amplitude a, wavenumber vector $\mathbf{k}$, and intrinsic frequency σ from the finite-depth dispersion relation,

$$\sigma = \sqrt{gk \tanh kD}\,, \tag{13}$$

where $k = |\mathbf{k}|$, $D = h + \eta^c$, h is the resting water depth. These quantities are specified at every horizontal grid point and time in the model integration from either a spectrum-peak (i.e., with only a single-component $\mathbf{k}$ or a superposition of a few wavenumber components) or a broadband (i.e., full-spectrum) wave field.

With the spectrum-peak approximation either the wave properties can be specified *a priori* or, more generally, from a WKB wave model that includes the CEW feedback (Appendices A and B). For a full-spectrum model with many $\mathbf{k}$ components, it is advantageous to represent the wave properties with a low number of wave variables to be shared with ROMS for memory exchange considerations (e.g., Kumar et al., 2012, 2017). Estimating the wave spectrum can be achieved using a spectral wave

https://doi.org/10.5194/egusphere-2026-2942
Preprint. Discussion started: 17 July 2026

model such as WW3 or SWAN (Booij et al., 1999), to cite only two. One-way coupling with ROMS is then performed by reading specific wave quantities as input for ROMS, saved from the output of the wave model.

In principle, full wave–current coupling with a spectrum wave model is possible but makes for an enormous calculation for realistic simulations. Even the most extensively coupled wave–current frameworks in the literature do not exchange the directional frequency spectrum itself between the wave and ocean models (Warner et al., 2010; Kumar et al., 2012; Couvelard et al., 2020); instead, a small set of bulk wave parameters (e.g., significant wave height, mean period and direction, surface Stokes drift and Stokes transport, breaking-induced TKE flux, Charnock parameter) is exchanged at coupling timesteps, and the vertical Stokes drift profile and other spectrally-dependent quantities required by the ocean-side wave-averaged equations are reconstructed internally from these bulk fields under simplifying assumptions about the underlying spectrum (e.g., the monochromatic-equivalent profile of Breivik et al. (2014); Breivik and Christensen (2020)). Full spectrum exchange is given no further consideration here, and we adopt a one-way configuration in which WW3 bulk output forces the ROMS-side NCWEC implementation.

3.1 Spectrum-peak waves

Because the monochromatic approximation of the spectrum-peak wave has already been presented in detail in U2010, we only briefly recall it here for completeness. The Stokes drift is expressed as

$$\mathbf{u}^{\mathrm{St}} = \frac{a^2\sigma}{2\sinh^2[\mathscr{H}]}\cosh[2\mathscr{Z}]\mathbf{k}\,, \tag{14}$$

and the Bernoulli head as

$$\mathscr{K} = \frac{1}{4}\frac{\sigma a^2}{k\sinh^2[\mathscr{H}]}\int_{-h}^{z}\partial^2_{z'}\mathscr{V}\sinh[2k(z-z')]dz'\,, \tag{15}$$

with a the mean wave amplitude, k the specturm-peak wavenumber, $\mathscr{H} = k(h+\eta+\hat{\eta}) = kD$, $\mathscr{Z} = k(z+h)$, and $\mathscr{V} = \mathbf{k}\cdot\mathbf{u}$.

The wave-averaged set-down is

$$\hat{\eta} = -\frac{a^2k}{2\sinh[2\mathscr{H}]}\,, \tag{16}$$

always negative, representing the depression of mean sea level seaward of the breakpoint. At the resolutions considered here ($dx > \mathcal{O}(10m)$) the surfzone is unresolved and the compensating set-up shoreward of the breakpoint is not captured.

The pressure correction term in the pressure continuity boundary condition is

$$\mathscr{P} = \frac{ga^2}{2\sigma}\left\{\frac{\tanh[\mathscr{H}]}{\sinh[2\mathscr{H}]}\left(-\partial_z\mathcal{V}|_{\eta^c} + \cosh[2\mathscr{H}]\partial_z\mathscr{V}|_{-h} + \int_{-h}^{\eta^c}\partial^2_{z'}\mathscr{V}\cosh[2kz']dz'\right) - 2k\tanh[\mathscr{H}]\mathscr{V}|_{\eta^c}\right\}. \tag{17}$$

This model is computationally economical because ROMS-NCWEC only requires a, $\mathbf{k}$, and σ as the wave input. Arguably, the spectrum-peak waves provide the most important WEC contribution for a circulation model.

https://doi.org/10.5194/egusphere-2026-2942
Preprint. Discussion started: 17 July 2026

3.2 Broadband waves

However, realistic surface wave fields have many energetic $\mathbf{k}$ components except under swell conditions. More generally, the spectrum-peak approximation underestimates the Stokes drift in mixed sea-swell conditions (Romero et al., 2021), motivating a broadband formulation for the conservative WEC terms for greater accuracy. To limit the size of the data transfer, this paper proposes a set of wave approximations for the Stokes drift, Bernoulli head, and quasi-static pressure,that represents with good fidelity the broadband wave spectra in wind-sea and swell conditions, building on previous work by Breivik et al. (2014) and Breivik and Christensen (2020).

The Stokes drift is approximated as

$$\mathbf{u}^{\mathrm{St}}(z) = \mathbf{u}_p^{\mathrm{St}}\mathcal{H} + \mathbf{u}_e^{\mathrm{St}}(1-\mathcal{H})\,, \tag{18}$$

where $\mathbf{u}_p^{\mathrm{St}}$ is the Stokes drift associated with the dominant and long wave component of the spectrum following a spectrum-peak formulation $\mathbf{u}_p^{\mathrm{St}}(z; H_s, k_p, \theta_p)$ of Eq. 14 using the spectrally weighted mean wave direction $\bar{\theta}$ and the peak wavenumber k_p. The tail of the wave spectrum represents short wind-generated waves, which contribute mostly to the surface, and are described by the Stokes drift $\mathbf{u}_e^{\mathrm{St}}$. It is a function of the full 2D (frequency and direction) wave spectrum Stokes drift surface value $\mathbf{u}^{\mathrm{St}}(z=\eta+\hat{\eta})$ and the Stokes transport U^{St}. The short period component is written as

$$\mathbf{u}_e^{\mathrm{St}} = \mathbf{u}^{\mathrm{St}}(z=\eta+\hat{\eta})\frac{\cosh 2k_e(z+h)}{\cosh 2k_e D}\,, \tag{19}$$

where k_e is an effective wavenumber computed as the ratio of the surface Stokes drift divided by twice the Stokes transport. The function $\mathcal{H}(z)$ smoothly connects the short and long components, it is

$$\mathcal{H} = \sqrt{\tanh\frac{|z|k_e}{2}}\,. \tag{20}$$

The Bernoulli head $\mathscr{K}$ is written as in the spectrum-peak approximation but using the filtered long-wave wave amplitude a_f and the peak wavenumber $\mathbf{k}_p = k_p(\cos\bar{\theta}, \sin\bar{\theta})$. The pressure correction $\mathscr{P}$ is re-written as function of the filtered long-wave wave amplitude a_f and k_p:

$$\mathscr{P} \simeq -G(\mathscr{K}_p,\sigma)a_f^2\partial_z\mathscr{V}|_\eta + G(\mathscr{K}_p,\sigma)a^2\cosh[2\mathscr{K}_p]\partial_z\mathscr{V}|_{-h} + G(\mathscr{K}_p,\sigma)a_f^2\int_{-h}^{\eta^c}\partial^2_{z'}\mathscr{V}\cosh[2k_p z']dz' - 2M(k_p,k_e)\mathbf{u}^{\mathrm{St}}\cdot\mathbf{u}|_{\eta^c}\,, \tag{21}$$

where $G(\mathscr{K}_p,\sigma) = \frac{g}{2\sigma}\frac{\tanh\mathscr{K}_p}{\sinh 2\mathscr{K}_p}$, $\mathscr{K}_p = k_p D$, and

$$M(k_p,k_e) = \frac{\sinh^2 k_e D}{\cosh 2k_e h}\tanh k_p h + \frac{\sinh^2 k_p D}{\cosh 2k_p h}(1-\tanh k_e h)\,. \tag{22}$$

The latter is a dimensionless function to insure the smooth blending of the deep and shallow water components. The set-down $\hat{\eta}$ is saved as the full spectral computation. The filtered long-wave wave amplitude a_f is computed by multiplying the total

https://doi.org/10.5194/egusphere-2026-2942
Preprint. Discussion started: 17 July 2026

wave amplitude by the ratio of the square root of the set-down from the full spectral computation and the one computed with the monochromatic approximation, see Eq. 16.

To use the broadband expressions in ROMS, one needs to use a wave model to resolve the six following fields: the total wave amplitude a, the peak wavenumber k_p, the spectrally-weighted mean wave direction $\bar{\theta}$, the surface Stokes drift $\mathbf{u}^{\mathrm{St}}(z=\eta+\hat{\eta})$, the Stokes transport $\mathbf{U}^{\mathrm{St}}$, and the set-down $\hat{\eta}$. Thus, in terms of data exchange, this approach is twice as heavy as the spectrum-peak approximation (Sec. 3.1), but it provides a gain in representational accuracy.

4 Non-Conservative WEC

In the equations of motion (1), the non-conservative WEC force $\mathbf{F}^w$ includes wave breaking (Sec. 4.1), bottom streaming (Sec. 4.2), and enhanced bottom drag (Sec. 4.3) and vertical mixing. We represent these effects in the momentum balance as an acceleration force $\mathbf{A}^w$ and extra vertical mixing $\mathbf{D}^w$:

$$\mathbf{F}^w = \mathbf{A}^w + \mathbf{D}^w \,, \tag{23}$$

where

$$\mathbf{D} + \mathbf{D}^w = \frac{\partial}{\partial z}\left(K_v^w \mathbf{u}_z\right) \,, \tag{24}$$

with $\mathbf{D} = \frac{\partial}{\partial z}(K_v^{cd}\mathbf{u}_z)$ the current-only vertical mixing and K_v^w the wave-enhanced turbulent viscosity. $\mathbf{A}^w$ is expressed in terms of a wave breaking component $\mathbf{B}^{wb}$ and a wave streaming one $\mathbf{B}^{str}$. These wave-induced accelerations can be written as body forces; alternatively, if the associated turbulent boundary layers are too thin to be resolved in a particular model configuration, these dissipation processes can be expressed as equivalent boundary stresses for $\mathbf{u}$. By making the vertical integral of the body force and the alternative boundary stress identical, the two formulations differ only through the vertical distribution of the forcing, which especially matters in the shallow surfzone. The body-force profile implemented here follows U2010 and was calibrated in shallow water, making it appropriate for surfzone-resolving configurations.[3]

For any non-conservative wave process (here either wave breaking or bottom drag), the wave-averaged force on currents takes the general form, $\mathbf{B} = \varepsilon^w f(z)\mathbf{k}/\rho\sigma$, where ε^w is the wave dissipation rate, $f(z)$ is a vertical shape function with unit integral, and $\mathbf{k}/\sigma$ is the inverse phase velocity for the dominant wave component. This relationship between wave dissipation and current force is derived from quasi-linear theory (QLT; McWilliams, 2026) and sometimes called the dissipative pseudomomentum rule. This relationship requires knowledge of ε^w from wave measurements or models.

The wave-enhanced vertical mixing vertically distributes the momentum injected at the surface by breaking with the surface boundary condition,

$$K_v^w \mathbf{u}_z = \tau^{wind} + \tau^{wb} \;\text{ at }\; z = \eta + \hat{\eta} \,, \tag{25}$$

[3]The distinction of body-force versus stress should not be conflated with the deep- versus shallow-breaking terminology used in the surfzone community (e.g. Marchesiello et al., 2021). These terms refer to the depth-induced surfzone breaking profile, where deep is depth-independent and shallow refers to surface-intensified profiles.

https://doi.org/10.5194/egusphere-2026-2942
Preprint. Discussion started: 17 July 2026

and at the bottom by the current drag and wave streaming with the bottom condition

$$K_v^w \mathbf{u}_z = \tau^{cd} - \tau^{str} \text{ at } \mathrm{z} = -\mathrm{h}\,, \tag{26}$$

where τ^{wind} is the surface wind stress (represents only tangential stress plus unresolved breaking), τ^{wb} is the surface stress due to depth-induced surfzone wave breaking (Sec. 4.1), τ^{str} is the bottom stress due to wave bottom frictional dissipation or wave streaming (Sec. 4.2), and τ^{cd} is the bottom stress due to current bottom drag which can be enhanced by waves (Sec. 4.3). The negative sign of τ^{str} in the bottom boundary condition represents the injection of momentum in the direction of wave propagation by bottom streaming. In the case where wave propagation is in the same direction as the bottom current, τ^{str} opposes the effects of τ^{cd}.

Adding to the current-only mixing, the incremental wave-enhanced momentum mixing is due to surface breaking near surface

$$\mathbf{D} + \mathbf{D}^w = \frac{\partial}{\partial z}\left[K_v^w(z)\mathbf{u}_z\right] = \frac{\partial}{\partial z}\left[\left(K_v^{wb}(z) + K_v^{cd}(z)\right)\mathbf{u}_z\right]\,, \tag{27}$$

and bottom current drag near bottom

$$\mathbf{D} + \mathbf{D}^w = \frac{\partial}{\partial z}\left[K_v^w(z)\mathbf{u}_z\right] = \frac{\partial}{\partial z}\left[K_v^{cd}(z)\mathbf{u}_z\right]\,, \tag{28}$$

noting that $K_v^{cd}(z)$ is not an explicit additive term but rather represents the enhancement of $K_v(z)$ within KPP due to the wave-modified friction velocity entering the bottom boundary layer computation.

We take care that no double counting of the wave momentum flux between τ^{wind} and τ^{wb} occurs. Following oceanic modeling convention, τ^{wind} is the surface wind stress from bulk flux parameterization, which implicitly includes the momentum flux from deep-water white-capping. τ^{wb} represents only the additional momentum flux from depth-induced surfzone breaking, which is not captured by the bulk formulae because it depends on the local bathymetry. Deep-water white-capping therefore contributes to momentum only through τ^{wind}, and to near-surface vertical mixing through K_v^{wb} (Sec. 4.1.2), without a separate momentum term. Depth-induced surfzone breaking contributes both as a momentum source (τ^{wb}) and to vertical mixing (K_v^{wb}).

4.1 Wave breaking

Breaking waves exert a stress on the wave-averaged currents and create an increase of near surface turbulence. Breaking can be depth-induced, in the surfzone, or wave slope-induced, i.e. white capping, which can happen in deep waters. In the presence of wave breaking, we consider that surface streaming due to molecular viscosity is negligible (because the wave-viscous surface boundary layer is ∼mm thick). We account separately for the momentum injection due to wave breaking (Sec. 4.1.1) and for the near surface incremental momentum mixing due to wave breaking (Sec. 4.1.2).

4.1.1 Breaking acceleration

Representation as a surface stress: For nearshore depth-induced breaking, the dissipation rate ε^{wb} (units $\mathrm{m^3 s^{-3}}$, energy units i.e., specific (divided by ρ_0) dissipation rate) drives a divergence of wave radiation stress that accelerates alongshore currents.

https://doi.org/10.5194/egusphere-2026-2942
Preprint. Discussion started: 17 July 2026

The surface stress associated with ε^{wb} is from ROMS variables alone.

$$\tau^{wb} = \varepsilon^{wb} \frac{\mathbf{k}_p}{\sigma}\,, \tag{29}$$

with $\mathbf{k}_p$ the peak wavenumber with the wave direction $\bar{\theta}$ and σ the cyclic wave frequency, written without surface roller here[4]. This stress is added to the wind stress at surface following Eq. 25 only nearshore.

Representation as a body force: Alternatively, the wave breaking momentum injection can be written as a body force (an acceleration) with a prescribed vertical distribution as follow

$$\mathbf{B}^{wb} = \varepsilon^{wb} \frac{\mathbf{k}_p}{\rho_0 \sigma} f^b(z), \tag{30}$$

where $f^b(z)$ is a downward decaying normalized vertical profile $f^b(z) = \cosh\left[k_b(z+h)\right]$. The breaking penetration scale is defined by $k_b^{-1} = 2ac_b$ where c_b is an $\mathcal{O}(1)$ constant set by default to 0.2 in ROMS, i.e. 20% of the rms wave height ($H_{\mathrm{rms}} = 2a$). Note that the relation to the equivalent surface stress in the previous section is $\tau^{wb} = \rho_0 D \overline{\mathbf{B}}^{wb}$ where the bar denotes a depth-averaging.

4.1.2 Breaking-induced vertical mixing

Wave breaking induces a bulk addition to the turbulent viscosity K_v near surface of K_v^{wb} for both for eddy viscosity and diffusivity. The incremental momentum mixing due to wave breaking can be expressed using the mean peak approximation or a the method proposed by Romero et al. (2021) which better represents deep water breaking. We recall both their expressions hereafter.

Spectrum-peak waves: The spectrum-peak wave approximation expresses the eddy viscosity and diffusivity due to wave breaking as

$$K_v^{wb}(z) = C_b \left(\frac{\varepsilon^{wb}}{\rho_0}\right)^{1/3} 2aD f^{Kv}(z) \tag{31}$$

where C_b is a constant directly controlling the magnitude of wave-breaking-induced vertical mixing (U2010 uses $C_b = 0.03-0.1$) and $f^{Kv}(z) = \cosh\left[k_{Kv}(z+h)\right]$ is a downward decaying normalized function $k_{Kv}^{-1} = 2ac_{Kv}$ with c_{Kv} is $\mathcal{O}(1)$, set by default to 1.2 in ROMS.

Broadband waves: Alternatively to using Eq. 31, Romero et al. (2021) parameterizes near-surface eddy viscosity and diffusivity from the TKE dissipation rate based on the near-surface observations by Sutherland and Melville (2015) to better account for both deep-water (whitecapping) and depth-limited breaking. The key conceptual difference with the monochromatic case which distributes breaking mixing over the full water column (appropriate for shallow surfzones), is that Romero et al. (2021) confines it near the surface (appropriate for deep-water breaking and applicable across all depths). The vertical viscosity and diffusivity are parameterized as follows:

$$K_v^{wb}(z) = \mathcal{T}(z') \left(\frac{\varepsilon^{wb}}{\rho_0 2\sqrt{2}a} \frac{E}{B + Cz' + Dz'^2}\right)^{1/3} \ell^{4/3}\,, \tag{32}$$

[4] Roller dynamics is used only for a surfzone-resolving configuration (Sec. B3.1).

https://doi.org/10.5194/egusphere-2026-2942
Preprint. Discussion started: 17 July 2026

defining the dimensionless depth $z' = (z - \eta - \hat{\eta})/(2\sqrt{2}a)$, and the tapering function $\mathcal{T}(z) = 1 - \tanh^4 z$ which smoothly kills $K_v^{wb}(z)$ at depth. The constants $B = 4/30$, $C = -8/3$, $D = 10/3$, and $E = 0.9508$ have been determined by fitting with observed TKE dissipation rates. Following Terray et al. (1999), the length scale ℓ follows a linear law,

$$\ell(z) = \begin{cases} \kappa z_{0s} & \text{if } |Z| \leq z_{0s} \\ \kappa |Z| & \text{otherwise} \end{cases} \tag{33}$$

where κ is the von Kármán constant and $Z = z - \eta - \hat{\eta}$ is the depth from the surface. The aerodynamic roughness length z_{0s} controls the mixing length scale near the surface and is proportional to the wave amplitude, and in ROMS set to $z_{0s} = 2\sqrt{2}c_{Kv}a$. But unlike with the mean peak approximation where C_b linearly scales the entire K_v^{wb} magnitude, with this formulation z_{0s} enters through the mixing length ℓ, making the dependence nonlinear ($\propto \ell^{4/3}$) (Moghimi et al., 2016).

Vertically averaged, this gives

$$\overline{K}_v^{wb} \sim C_b \times 2\sqrt{2}a \left(\frac{\varepsilon^{wb}}{\rho_0}\right)^{1/3}, \tag{34}$$

which differs from the vertical integration of Eq. (25) in its dimensional scaling: Romero et al. (2021) yields $\overline{K}_v^b \propto a$ (one length scale), whereas U2010 yields $\overline{K}v^b \propto a \cdot D$ (a product of two length scales). The two expressions agree only at a single depth $D = 0.1\sqrt{2}/C_b$. The U2010 scaling is appropriate in the surfzone where $D \sim \mathcal{O}(a)$, but overestimates depth-averaged mixing under deep-water white-capping where $D \gg a$, a consequence of the underlying Battjes (1975) formulation being designed specifically for surfzone conditions. Romero et al. (2021) confines mixing to a near-surface layer of thickness proportional to a, making it applicable to both deep-water white-capping and depth-induced surfzone breaking. Note that this formulation is not double counting the wind stress as it does not contain an equivalent deep water stress. The use of this parameterization is expected to decrease surface vorticity (and surface current gradients in general) in deep-water (Romero et al., 2021).

4.2 Wave-induced bottom streaming

4.2.1 Relation between wave-induced bottom streaming and wave-enhanced bottom drag

Physically, wave-induced bottom streaming and wave-enhanced bottom drag share a common origin. Both arise from the interaction of wave orbital motions with the solid bottom boundary. The QLT demonstrates that the same quadratic drag force produces, upon wave averaging, both a streaming acceleration through the wave vortex force and an enhanced drag on the mean current (McWilliams, 2026). The streaming transfers momentum in the wave propagation direction proportional to $\varepsilon^{str}\mathbf{k}_p/\sigma$, while the enhanced drag opposes and redirects the mean current with a different dependence on wave and current properties. In ROMS-NCWEC, these two effects follow separate computational pathways, reflecting the different vertical resolution requirements of each. The streaming is computed from ε^{str} via the dissipative pseudomomentum relationship (Sec. 4.2.2), expressible as a bulk stress without resolving the wave bottom boundary layer (WBBL). The wave-enhanced drag cannot be computed directly from QLT because doing so would require resolving the wave boundary layer, typically only centimeters thick and unresolvable on the model grid. Instead, the Soulsby (1995) empirical parameterization is used (Sec. 4.3), modifying the current

https://doi.org/10.5194/egusphere-2026-2942
Preprint. Discussion started: 17 July 2026

drag coefficient based on the ratio of wave-to-current bottom stresses, a formulation widely validated against laboratory and field measurements (Soulsby et al., 1993).

4.2.2 Streaming force

Representation as a bottom stress: The wave bottom dissipation (due to molecular viscosity) is noted ε^{str} (units: $\mathrm{m^3 s^{-3}}$). It generates bottom streaming within the bottom boundary layer. Following the dissipative pseudomomentum rule, the bottom stress formulation is

$$\tau^{str} = \varepsilon^{str}\frac{\mathbf{k_p}}{\sigma}. \tag{35}$$

When the WBBL, typically only a few cm, is too thin to be resolved on the model grid, then the streaming acceleration is applied only as a stress in the bottom grid cell. This formula implies bottom streaming occurs in the direction of wave propagation. In the surfzone, near-bed undertow opposite to the incident waves dominates over streaming. The wave streaming is important in the inner-shelf (more about this in Sec. 6) and can create a near-bottom convergence zone where it meets the undertow (Wang et al., 2020).

Representation as a body force: The wave streaming can be written as a body force (as opposed to a bottom stress) as follow

$$\mathbf{B}^{str} = \varepsilon^{str}\frac{\mathbf{k_p}}{\rho_0\sigma}f^{wd}(z), \tag{36}$$

where $f^{wd}(z)$ is an upward decaying normalized vertical profile. The chosen vertical shape is $f^{wd}(z) = \cosh\left[k_{wd}(\eta^c - z)\right]$ with $k_{wd}^{-1} = c_{wd}\delta_w$. The dimensionless factor c_{wd} depends on the wave spectrum: For theoretical turbulence $c_{wd} = 1$ whereas $c_{wd} = 3$ fits laboratory measurements of random waves (Klopman, 1994; Reniers et al., 2004), which is the value we retain by default in current ROMS. The WBBL thickness is

$$\delta_w = 0.09 k_N \left(\frac{a^w_{orb}}{k_N}\right)^{0.82}, \tag{37}$$

where $a^w_{\mathrm{orb}} = |\mathbf{u}^w_{\mathrm{orb}}|/\sigma$ is a semi-orbital excursion of short waves and $k_N = 30 z_0$ is the Nikuradse roughness. Note that the relation to the equivalent surface stress in Eq. (29) is $\tau^{str} = \rho_0 D \bar{\mathbf{B}}^{str}$ from depth integration.

4.3 Wave-enhanced bottom drag

Interactions of waves and currents near the bottom boundary increase the bottom stress τ^{cd} felt by the mean currents above the boundary layer. In ROMS, τ^{cd} is computed through the current drag coefficient. where wind stress for instance is applied explicitly, the bottom boundary in ROMS relies on a drag law relating the bottom stress to the velocity at the lowest resolved grid level. This is because the turbulent bottom boundary layer is typically too thin to be resolved on the model grid, and the drag coefficient parameterizes the unresolved near-bed velocity shear.

The waves enhance the current bottom drag stress following the empirical formula of Soulsby (1995):

$$\tau^{cd} = \tau_c\left[1 + 1.2\left(\frac{|\tau_w|}{|\tau_w| + |\tau_c|}\right)^{3.2}\right], \tag{38}$$

https://doi.org/10.5194/egusphere-2026-2942
Preprint. Discussion started: 17 July 2026

(a completely different functional form from the QLT derivation (McWilliams, 2026)) where τ_c is the non-wave current bottom drag in a log-layer:

$$\tau_c = \rho_0 \left[\frac{\kappa}{\ln z_m/z_0}\right]^2 |\mathbf{u}|\mathbf{u} = \rho_0 r_D \mathbf{u}\,, \tag{39}$$

introducing r_D the drag coefficient and z_0 the seabed roughness, and

$$\tau_w = 0.5\rho_0 f_w |\mathbf{u}^w_{orb}|^2\,, \tag{40}$$

with the wave friction factor

$$f_w = 1.39\left(\frac{\sigma z_0}{|\mathbf{u}^w_{\text{orb}}|}\right)^{0.52}\,. \tag{41}$$

τ_c and τ_w are bottom drag stresses due to current and waves respectively, z_m is a reference depth above the bed, nominally equivalent to a half bottom-most grid cell height. barotropic model, i.e. if not using SOLVE3D, $z_m = D/2$). So the wave-enhanced drag has two components: The first term opposes the mean current directly. The second term projects the current onto the wave direction and opposes that component, which means it acts to reduce the current component aligned with wave propagation. This formulation from Soulsby (1995) provides a direct empirical parameterization of the mean enhanced bottom stress through a multiplicative factor depending on the ratio of wave-to-current stresses (Eq. 38). It is currently the only option available in the code. Alternative bottom drag laws exists, e.g. from Feddersen et al. (2000), which uses nonlinear velocity moment closures $\langle|\mathbf{u}|u\rangle$ rather than a direct stress enhancement, when both mean currents and oscillatory wave motions contribute to the near-bed velocity field. Other alternatives can be seen in the COAWST code (Kumar et al., 2012) implemented wave-enhanced bottom drag based on Madsen (1994) wave-current boundary layer models, which explicitly resolve the wave boundary layer structure. Their orbital velocity $\mathbf{u}^w_{\text{orb}}$ is provided by SWAN using a monochromatic approximation.

4.4 General bottom boundary layer thickness criterion

Wave streaming enhances the vertical shear and near-bottom turbulence in the inner shelf hence the bottom boundary layer thickness increases. KPP determines the BBL thickness h_{BBL} based on the first depth (starting from $z = -h$) at which $Cr(z) = 0$ with

$$Cr(z) = \int_z^0 J(z')\left[\left(\frac{\partial \mathbf{u}}{\partial z}\right)^2 - \frac{N^2(z)}{Ri_c} - C_{ek} f^2\right] dz' + \frac{V_t^2(z)}{|z|} = I_{\text{int}} + \frac{V_t^2(z)}{|z|}\,, \tag{42}$$

where $J(z) = |z|/\left(|z| + \epsilon h_{BBL}\right)$

We propose a modification of $Cr(z)$ to account for the impact of bottom streaming on the bottom boundary layer thickness such as

$$Cr(z) = I_{\text{int}} + \frac{V_t^2(z)}{|z|} + \alpha (u_*^{wstr})^2 \frac{|z|}{h} \tag{43}$$

https://doi.org/10.5194/egusphere-2026-2942
Preprint. Discussion started: 17 July 2026

where $(u_*^{wstr})^2 = |\tau^{wd}|$ is the friction velocity due to wave streaming. By design, we choose α such that under rotation and streaming alone yields $h_{BBL} = 1$ m, making the resulting criterion independent of streaming intensity. This prescribed floor serves two purposes: it ensures that streaming and rotational effects are communicated to at least one sigma layer above the bed, and it prevents the bulk Richardson criterion from collapsing the BBL below the vertical grid resolution in shallow, weakly stratified water. The choice of 1 m is consistent with the physical bottom Ekman depth $\delta_E^{\rm bot} \sim \kappa u_*^{\rm bot}/f$, where $u_*^{\rm bot} = \sqrt{|\tau^{cd}|/\rho_0}$ is the friction velocity from the log-layer bottom drag (Sec. 4.3) and τ^{cd} is the bottom stress, which remains $\mathcal{O}(1\text{–}10)$ m under typical inner-shelf conditions.

Enforcing a 1 m BBL thickness under rotation and streaming alone determines α as

$$\alpha = \frac{C_{ek} f^2}{(u_*^{wstr})^2} \frac{h}{|-h+1|} \left(1 + \epsilon \log\left(\frac{\epsilon + |-h+1|}{\epsilon + |-h|}\right)\right) . \tag{44}$$

upon which u_*^{wstr} cancels by construction, and the additional term in Eq. (43) reduces to

$$\alpha (u_*^{wstr})^2 \frac{|z|}{h} = C_{ek} f^2 \frac{|z|}{|-h+1|} \left(1 + \epsilon \log\left(\frac{\epsilon + |-h+1|}{\epsilon + |-h|}\right)\right) . \tag{45}$$

depending only on the Coriolis frequency and water depth. For $\epsilon \ll 1$, it reduces to $C_{ek} f^2 \frac{|z|}{h-1}$. This term is most impactful when wave streaming is important but shear and stratification are relatively weak, the inner-shelf regime where streaming is dynamically relevant (Sec. 6.1.1) and the water column is typically shallow and well-mixed, but not yet dominated by the strong vertical shear of the breaking zone.

4.5 Wave variables required for non-conservative WEC

For ROMS-NCWEC to run, the model needs from a wave model:

- the breaking dissipation (ε^{wb}),
- the frictional dissipation (ε^{str}),
- the orbital velocity amplitude ($u^w_{\rm orb}$; optional). By default, the orbital velocity amplitude is computed via the spectrum-peak expression $|\mathbf{u}^w_{\rm orb}| = \sigma a / \sinh kD$ but if available one should be reading in the spectrally integrated offline orbital velocity from WW3 (accuracy gain), better representing the broadband wave field, with main differences nearshore,

in addition to the wave variables required for the conservative WEC (listed in Sec. 3). The seabed roughness z_0 is set in an input file.

5 Model validation: Replicating Duck 1994

5.1 Velocities and vertical eddy viscosity

The Duck94 field experiment at the U.S. Army Corps FRF, Research Facility Duck, North Carolina, provides a well-established benchmark for nearshore wave-current interaction models (Faria et al. 1998, 2000, and subsequent studies). We focus on

https://doi.org/10.5194/egusphere-2026-2942
Preprint. Discussion started: 17 July 2026

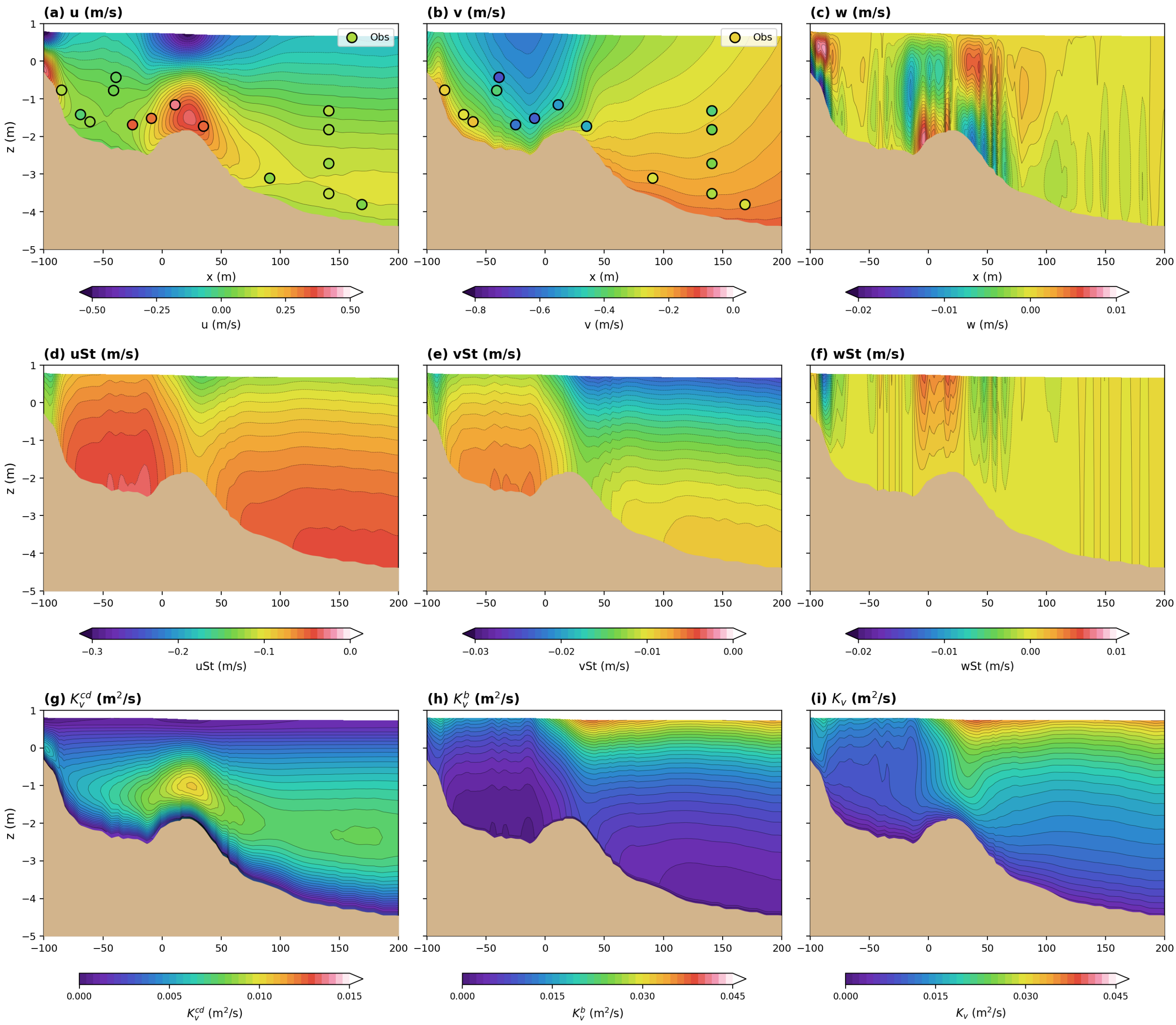

Figure 1. Cross-shore profiles of (a) u, (b) v, (c) w (m/s), (d) u^{St}, (e) v^{St}, and (f) w^{St} (m/s), (g) K_v^{cd}, (h) K_v^{wb}, and (i) $K_v = K_v^{cd} + K_v^{wb}$, (m^2/s), 6hrs after initialization. In (a) and (b) are scattered the time-averaged velocities from the fixed array (v03-v05, v12-v15, v17-v19, 10 sensors, one per x), the stationary sled (v21/v24, v22/v25 at $x \sim -40$m, 2 unique heights, duplicates averaged) and the vertical stack (v41/v46, v42/v47, v43, v44 at $x \sim 140$m, 4 unique heights) of the Duck 1994 experiment (the 8m depth array (v8x at $x \sim 654$m) was excluded).

https://doi.org/10.5194/egusphere-2026-2942
Preprint. Discussion started: 17 July 2026

October 12, 1994, a period of strong obliquely-incident storm waves that drive a well-developed alongshore jet within the surf zone. The measurements comprise a stationary vertical stack of four electromagnetic current meters at $x \sim 140$ m, a stationary sled with two measurement heights at $x \sim -40$ m, and a fixed cross-shore array of near-bed sensors spanning the surf zone, as well as cross-shore pressure sensor arrays (Fig.1 a-b). The CRAB-mounted traversing profiles used by Faria et al. (1998, 2000) are not included in the present dataset. For each sensor, 3-hour mean velocities from three Oct 12 runs (0700, 1000, 1300 EST) are averaged with equal weight and converted from the FRF sign convention (u shoreward, v southward, cm/s) to the ROMS convention (u offshore, v northward, m/s). Further details of the fixed-array data acquisition are given in Gallagher et al. (1998); Feddersen et al. (1997); the current meter time series are archived at https://zenodo.org/records/8286253.

U2010 first produced a ROMS configuration to compare to these Duck94 observations. They performed sensitivity experiments to the parameters of breaking, streaming and bottom drag, using the WKB model with and without CEW. With ROMS-NCWEC, we reproduce here a configuration close to the configuration of Run 8 from U2010 but with offline wave forcing: That is a 2D vertical cross-shore section assuming alongshore uniformity, with periodic alongshore boundary conditions. The domain has $dx = 2$ m cross-shore resolution and 32 vertical s-levels. The wave forcing file is provided by the COAWST Duck94 test case,[5] providing offline wave forcing consistent with the observed conditions. The simulation is unstratified, forced by analytical wind stress and offline spectrum-peak wave forcing (no CEW, no roller) including breaking and wave drag dissipation. The Soulsby (1995) wave-enhanced bottom drag is used with $z_0 = 0.001$ m. Breaking and streaming are applied as a 3D body forces, using $c_b = 0.2$, $c_{wd} = 3.0$, and breaking-induced mixing follows U2010 with $c_{Kv} = 1.2$ and $C_b = 0.03$. The simulation is initialized from rest, with 0.7 m elevation and integrated for 6 hours to reach steady state.

The model recovers the essential nearshore flow features (see Fig. 1): the surf-zone overturning circulation with onshore surface flow and offshore near-bed undertow (Fig. 1 a), and the alongshore current peaking shoreward of the bar (Fig. 1 b). Vertical velocity (Fig. 1 c), Stokes drifts (Fig. 1 d,e,f) and vertical viscosity (Fig. 1 g,h,i) are all recovered consistent with U2010. Normalized RMS errors against the 20 current meter positions (plotted in Fig. 1 a and b) are 0.195 for cross-shore velocity and 0.309 for alongshore velocity. These errors fall within the range reported by U2010, where u_{error} and v_{error} span 0.43-0.87 and 0.08-0.56 respectively across their sensitivity experiments (against 42 current meter positions; fixed-array + CRAB/mobile-sled), and are comparable to the Newberger and Allen (2007) results (u_{error} =0.45-0.70, v_{error} =0.12-0.50). Noting that our simulation has better cross-shore (u) fit but using less points of comparison (20 against 42). We also reproduce a configuration using WKB (and CEW) which normalized RMS errors are 0.264 for cross-shore velocity and 0.488 for alongshore velocity, also within range. This agreement, obtained without lateral momentum diffusion (in contrast to U2010 who used non-zero diffusion) and with the extra treatment of the bottom boundary layer, lends confidence in the non-conservative WEC implementation in the modern UCLA ROMS codebase and provides a foundation for the regional application that follows (in Sec. 6).

[5]The NetCDF file `duck_02132011.nc` available at `https://github.com/DOI-USGS/COAWST/tree/main/Projects/Ducknc`.

https://doi.org/10.5194/egusphere-2026-2942
Preprint. Discussion started: 17 July 2026

5.2 Horizontal momentum balance

We further validate the dynamics of the Duck94 solution in ROMS-NCWEC by analyzing the depth-integrated horizontal momentum balance, following U2010. Integrating the momentum equation (Eq. 1) over depth in the xi direction (the ROMS curvilinear horizontal coordinates are xi,eta) yields the budget:

$$\partial_t \overline{u} = \underbrace{-\overline{\partial_x(\phi^c)}}_{\text{(PGF) Modified pressure gradient force}} \tag{46}$$

$$\underbrace{-\overline{f\,v} - \overline{f\,v^{\mathrm{St}}}}_{\text{(Cor) Coriolis + Stokes-Coriolis}} \tag{47}$$

$$\underbrace{-\overline{[(\mathbf{u}+\mathbf{u}^{\mathrm{St}})\cdot\nabla_\perp]u + (w+w^{\mathrm{St}})\partial_z u}}_{\text{(Adv) Lagrangian advection}} \tag{48}$$

$$\underbrace{+\overline{\mathrm{hvf}_x}}_{\text{(HVF) Reduced horizontal vortex force}} \tag{49}$$

$$\underbrace{+\tau_x^{wind}}_{(\tau\text{ wind) Wind stress}} \tag{50}$$

$$\underbrace{+\tau_x^{wb}}_{(\tau\text{ wb) Wave breaking stress}} \tag{51}$$

$$\underbrace{+\tau_x^{str}}_{(\tau\text{ str) Streaming stress}} \tag{52}$$

$$\underbrace{-r_D\,u\big|_{-h}}_{\text{(Bdrag) Bottom drag}} \tag{53}$$

$$\underbrace{+(\bar{u}^{2D} - \overline{u}^{3D})\cdot D/\Delta t}_{\text{(cpl) Barotropic–baroclinic (2D/3D) coupling correction}} \tag{54}$$

$$\underbrace{+\overline{\mathcal{D}_\perp}}_{\text{(Ndiss) Numerical dissipation}} \tag{55}$$

$$\underbrace{+\overline{\nabla_\perp\cdot(\nu_h\,\nabla_\perp u)}}_{\text{(Hmix) Horizontal mixing}} \tag{56}$$

With similar expression along eta. The reduced horizontal vortex force is

$$\mathrm{hvf}_x = J_x + \underbrace{(\mathbf{u}^{\mathrm{St}}\cdot\nabla_\perp)u + w^{\mathrm{St}}\partial_z u}_{\mathtt{St\ Adv}} \underbrace{-f\,v^{\mathrm{St}}}_{\mathtt{St\ Cor}} = u^{\mathrm{St}}\frac{\partial u}{\partial x} + v^{\mathrm{St}}\frac{\partial v}{\partial x}\,, \tag{57}$$

https://doi.org/10.5194/egusphere-2026-2942
Preprint. Discussion started: 17 July 2026

and similarly

$$\mathrm{hvf}_y = u^{\mathrm{St}}\frac{\partial u}{\partial y} + v^{\mathrm{St}}\frac{\partial v}{\partial y}\,. \tag{58}$$

In this budget, all the tendencies on the right-hand side should exactly cancel the left-hand side and in practice we verify that the residual is small. Term (46) is the modified pressure gradient force (PGF). It is determined by computing the hydrostatic relation Eq. (2) along with the surface condition Eq. (6). The term (47) is the Coriolis term (Cor), in Lagrangian form, i.e. including the wave-induced Stokes-Coriolis term (St Cor). Term (48) is the horizontal advection term (Adv), also in Lagrangian form, including both Eulerian and Stokes drift contributions. Term (49) is the reduced form of the horizontal vortex force (HVF), combining J of Eq. 4 with the Stokes drift horizontal advection (St Adv) and the Stokes-Coriolis term (St Cor) per Eq. (57-58). Upon vertical integration, there is no vertical advection term and the full vertical mixing integral reduces to its boundary values: the surface wind stress (50), the surface wave breaking (51), the bottom wave streaming (52), and the wave-enhanced bottom drag (53). If not using the stress framework, the terms (51) and (52) are replaced by the vertical integral of their respective body force expressions per Eq. (24) and (30). Term (54), the barotropic-baroclinic (2D/3D) coupling correction, vanishes when the barotropic-baroclinic splitting is well converged. Term (55) is the hyperdiffusion term of the order 3 upstream vertical scheme. Term (56) is the horizontal mixing (set to zero in this configuration).

The steady-state Duck94 solution recovers the classic surfzone momentum balance of U2010, as shown in Fig. 2. In the cross-shore direction (panel a), the primary balance is between the pressure gradient force (PGF), driven by wave set-up, and breaking, with bottom drag and advection acting as secondary corrections. In the alongshore direction, the uniform coastline geometry eliminates any PGF, so the primary balance is between bottom drag opposing the breaking plus the Lagrangian advection (τ^{wb} + Adv). The alongshore current is thus driven by oblique wave forcing and arrested by bottom drag, with wind stress and streaming as minor corrections. In the alongshore, the reduced HVF is exactly zero (Fig. 2d), a geometric consequence of the alongshore-uniform beach ($\partial/\partial y = 0$ in Eq. (58) has both $\partial u/\partial y$ and $\partial v/\partial y$ vanish). Horizontal diffusion is exactly zero since no explicit diffusion was applied (term 56). The residual, computed as the left-hand side minus the sum of all right-hand side terms, is negligible, confirming momentum budget closure.

This balance will serve as a useful baseline for the regional momentum balance analyzed in Sec. 6.

https://doi.org/10.5194/egusphere-2026-2942
Preprint. Discussion started: 17 July 2026

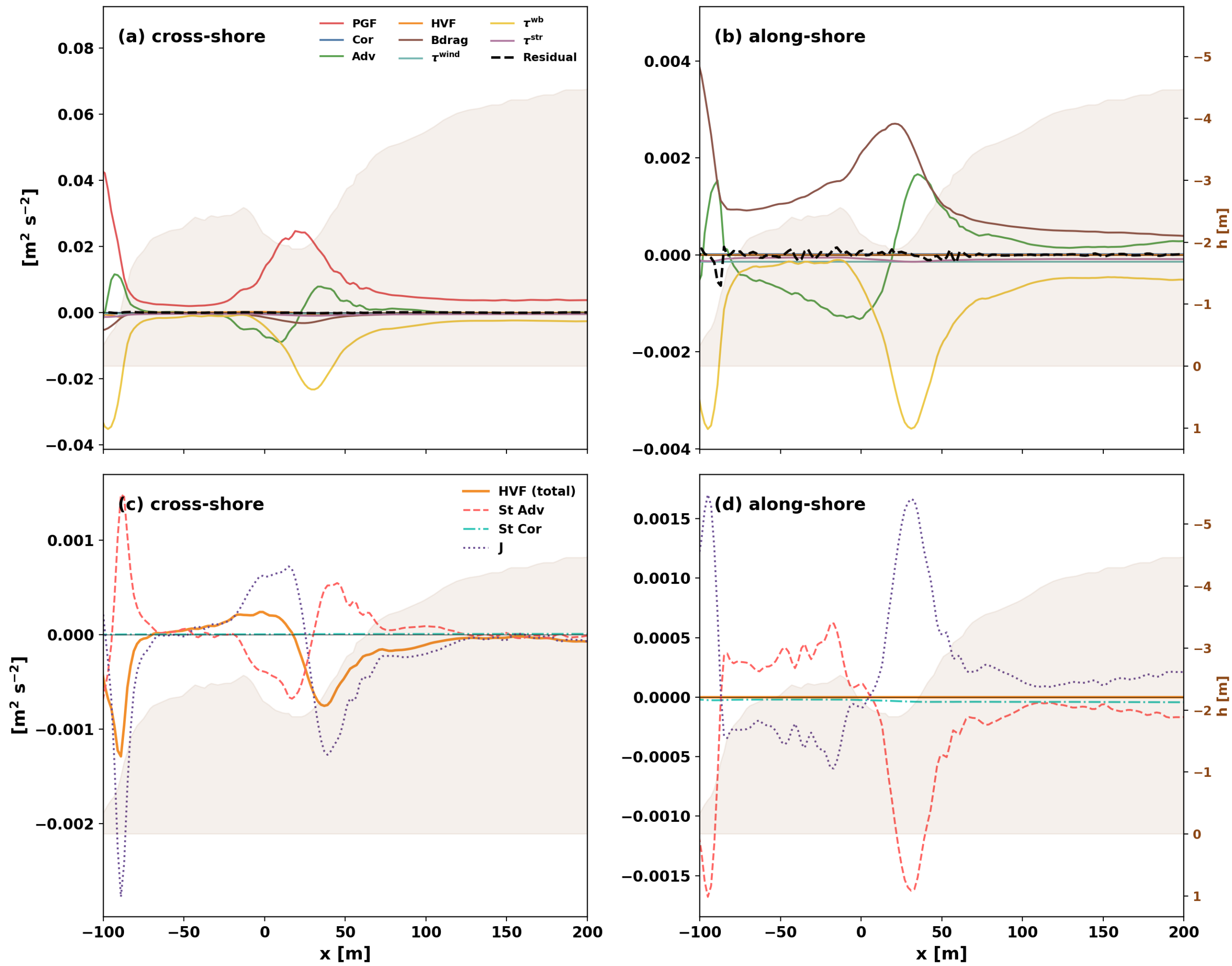

Figure 2. Depth-integrated (a) cross-shore and (b) alongshore momentum tendencies [m^2.s^{-2}] in the Duck94 ROMS replicate. The residual is the difference between $\partial_t \overline{u}$ and the sum of all the RHS terms (46) to (56). y-axis on the right shows the water depth (brown shading). Terms in the alongshore direction are one order of magnitude smaller than in the cross-shore direction. Cross-shore (c) and alongshore (d) depth-integrated horizontal vortex force decomposition: HVF is the sum of the vortex force J, the Stokes drift advection (St Adv) and the Stokes-Coriolis term (St Cor).

6 Regional demonstration: Point Arguello, CA

In this section, we explore ROMS-NCWEC in realistic settings. We focus on the region near Pt. Arguello south of Pt. Purisima and north of Pt. Conception, California, a coastline exposed to northwest swells with frequent mixed-sea states in winter. The grid is 1024×770 (see Fig. 3 for spatial extent) and 128 sigma levels. The boundary conditions and initial states are

https://doi.org/10.5194/egusphere-2026-2942
Preprint. Discussion started: 17 July 2026

inherited from a $dx = 100$m Central California simulation presented in Hypolite et al. (2021) and include the main 10 tidal constituents. The atmospheric forcing fields are interpolated from a California WRF 6km solution. WW3 is run independently at 300m (Romero et al., 2020) and the variables identified in Sec. 3.2 and Sec. 4.5 are interpolated onto the target ocean grid horizontal resolution $dx = 30$m (bathymetry via SRTM30+, Becker et al. (2009)). At 30m, this configuration is far finer than typical regional ocean circulation models yet remains insufficient to explicitly resolve the surfzone, motivating the nearshore boundary treatment described next.

6.1 Surf-permitting wave forcing

In nature, wave amplitude vanishes nearshore as waves break in shallow water. At coarse resolution, however, the surfzone is unresolved and wave amplitude may remain spuriously finite all the way to the coast in the WW3 solution. This causes wave quantities such as the set-down to diverge in ROMS, yielding CFL violations and sometimes simulation blow-up. Indeed, in shallow water where h vanishes, the Taylor expansion of Eq. (16) gives

$$\hat{\eta} \sim -\frac{a^2}{4(h+\eta+\hat{\eta})}\,, \tag{59}$$

showing that for $\hat{\eta}$ to remain bounded nearshore, a must vanish at the same rate as h, i.e. $a \sim \mathcal{O}(h)$. This problem is compounded with unseen sheltering and refraction nearshore along coastlines with small-scale headlands, embayments etc.

To reflect the natural wave amplitude decay nearshore, and allow the spatiotemporal smoothness of ROMS solutions, we impose an arbitrary linear decrease of the wave amplitude as a function of the bathymetry in the WW3 forcing file:

$$\mathrm{Where} \quad \mathrm{h} < \mathrm{H} \quad \mathrm{then} \quad \mathrm{a} \longrightarrow \frac{\mathrm{h}}{\mathrm{H}}\mathrm{a(H)}\,, \tag{60}$$

i.e. where H is a threshold depth below which the taper is applied. Since Stokes drift and wave dissipation are both proportional to a^2, the amplitude reduction naturally implies a $(h/H)^2$ scaling for both quantities. For wave breaking dissipation, the scaling could arguably be steeper since the breaking fraction also depends on a/h, but we retain $(h/H)^2$ for simplicity and consistency across all wave forcing terms. Note that, since h does not actually reach zero anywhere in ROMS ($h_{\min} = 3$ m), neither does the wave amplitude or WEC variables so this treatment does not generate any singularity.

Physically, this tapering achieves what depth-induced breaking would naturally produce at sufficient resolution: a progressive decay of wave amplitude toward the coast. Naturally resolving depth-induced breaking requires O(1–5m) wave model resolution, placing this limitation in the KPP grey zone for turbulence closure (Wyngaard, 2004; Chen et al., 2025), a fundamental constraint of the present class of regional coupled models. The tapering is therefore not arbitrary in purpose, though it is in form. The linear h/H dependence is the simplest choice satisfying the boundedness requirement, but it is not a calibrated parameterization of the breaking process. Because all wave variables are tapered consistently, the momentum balance within the tapering zone remains internally self-consistent: the terms relate to each other correctly even if their absolute magnitudes and horizontal gradients are not physically calibrated. Spatial diagnostics within the tapering zone should therefore be interpreted in terms of the sign and dominance of momentum balance terms rather than their precise horizontal structure.

https://doi.org/10.5194/egusphere-2026-2942
Preprint. Discussion started: 17 July 2026

With this treatment, a coarse-resolution model can be inner-shelf resolving and surfzone permitting, meaning it is not a surfzone model, but an inner-shelf model with a numerically stable and physically motivated nearshore boundary treatment.

6.1.1 Nearshore WEC spatial structure

With the above-mentioned treatment using $H = 30\,\mathrm{m}$, we configure two ROMS runs: a control without waves (NOWEC) and a wave-forced run (WEC) including the non-conservative effects described in Sec. 3. The two configurations share identical boundaries, initial state, and atmospheric forcing, differing only in the WEC compilation options (see Appendix A). Both are run through December 2006 and saved hourly. During this period, a notable long-period northwest swell reaches the coast between the 10th and the 15th with little concurrent wind, providing a range of dynamical regimes. We show results from a WEC configuration that uses the stress representation for both wave breaking and bottom streaming; an alternative implementation using body forces yields indistinguishable results at the grid scale.

The threshold $H = 30\,\mathrm{m}$ is chosen to lie seaward of the breaking zone as identified from the coarse WW3 solution, deliberately avoiding any coincidence between the tapering boundary and the region of active breaking. The absence of any anomalous feature in the solution at the 30 m isobath lends confidence that the tapering smoothly reduces wave amplitude in the nearshore rather than introducing artificial dynamics at the transition depth.

Fig. 3 illustrates the diversity of WEC-driven (conservative and non-conservative) surface vorticity structures across three snapshots spanning distinct forcing conditions.

https://doi.org/10.5194/egusphere-2026-2942
Preprint. Discussion started: 17 July 2026

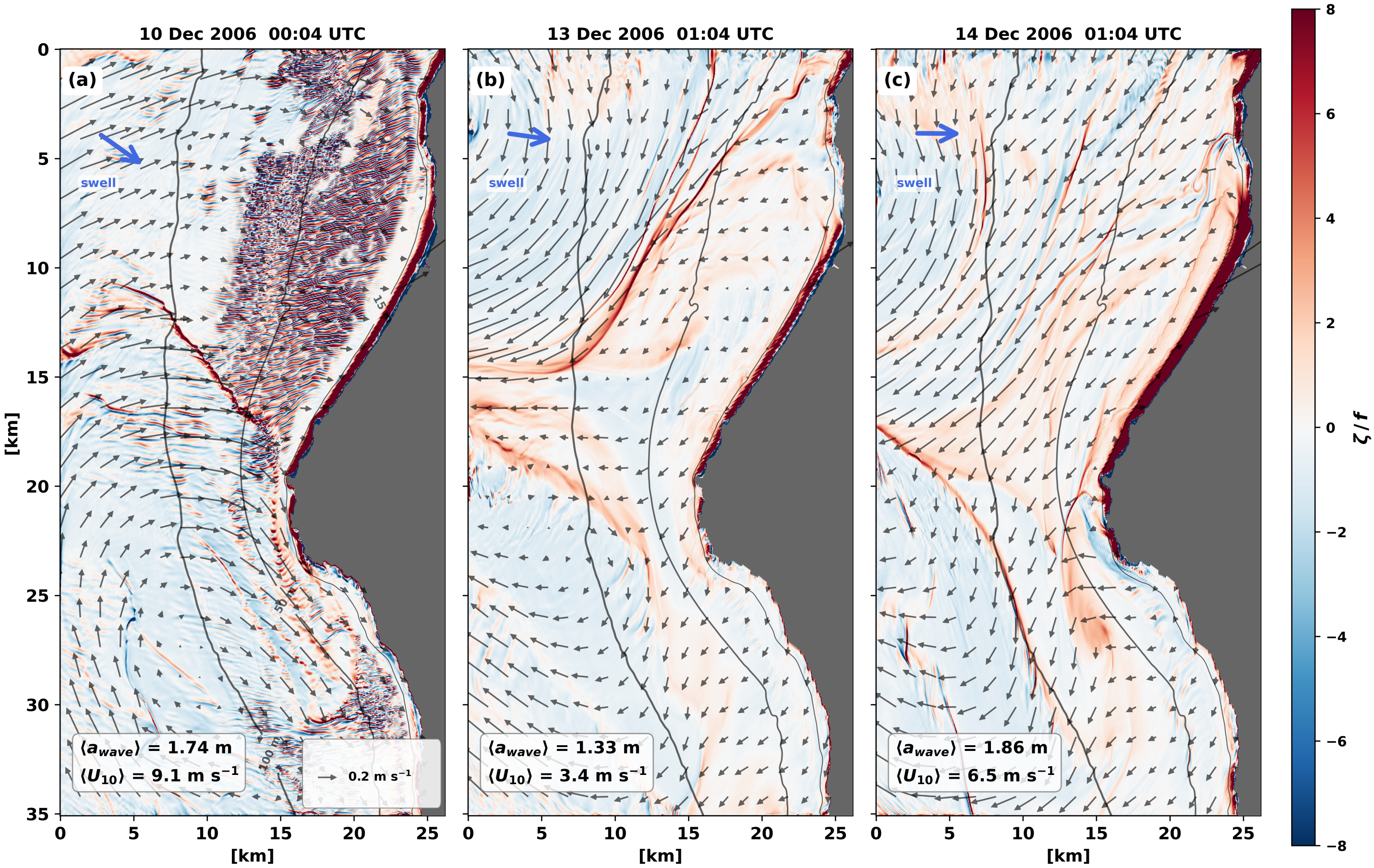

Figure 3. Surface normalized vorticity ζ/f at three ocean times of varying offshore-averaged wave amplitude $\langle a_{\mathrm{wave}}\rangle$ and 10-m wind speed $\langle U_{10}\rangle$. Surface horizontal velocity (black arrows). Mean swell propagation direction (blue arrow). Isobaths are at 15, 50, and 100 m (black contours).

In panel (a), high wind ($9.1\,\mathrm{m\,s^{-1}}$) combined with large swell ($\langle a_{\mathrm{wave}}\rangle = 1.74\,\mathrm{m}$) produces roll cells via the conservative vortex force (Hypolite et al., 2023), visible as alternating cyclonic/anticyclonic vorticity rolls oriented perpendicular to the coast, alongside an intense nearshore breaking band. In panel (b), calm wind ($3.4\,\mathrm{m\,s^{-1}}$) and moderate swell yield a classic submesoscale regime exemplified by a strain-induced front in the northern half of the domain with surface currents showing frontogenetic confluence. In panel (c), moderate wind ($6.5\,\mathrm{m\,s^{-1}}$) and larger swell ($\langle a_{\mathrm{wave}}\rangle = 1.86\,\mathrm{m}$) produce a wave-breaking regime: a strong band of cyclonic vorticity ($\zeta/f > 1$, red) is concentrated along the exposed coastline, and the surface velocity field shows a sharp shear between the offshore current and the wave-driven nearshore flow. The 15 m isobath sits at the seaward edge of this breaking zone.

https://doi.org/10.5194/egusphere-2026-2942
Preprint. Discussion started: 17 July 2026

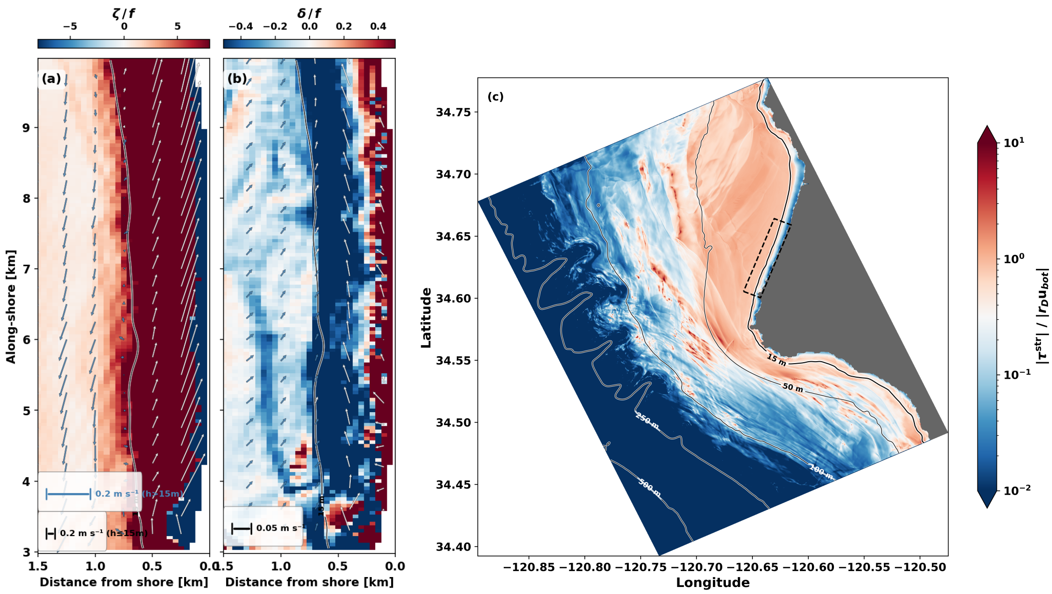

Figure 4. *Left*: Rotated nearshore cross-section (44° CCW, 14 Dec 2006 01:04 UTC). Surface ζ/f (a) and bottom δ/f (b). Velocity vectors: blue ($h > 15\,\mathrm{m}$), white ($h \le 15\,\mathrm{m}$). Scale bars bottom-left. 15 m isobath (white line). c: Ratio $\mathcal{R} = |\tau^{str}|/|r_D u_{\mathrm{bot}}|$ of wave streaming to bottom drag stress. Isobaths at 15, 50, 100, 250, 500 m (black). Ocean time is 14 Dec 2006 01:04 UTC (same as panel c in Fig. 3).

Fig. 4 zooms into the nearshore region of panel (c) and provides a dynamical interpretation of the wave-forced bottom flow.

Surface (a): The strong alongshore jet just inshore of the 15 m isobath creates a sharp lateral shear zone, with fast flow nearshore and slower flow offshore, generating cyclonic vorticity ($\zeta/f > 0$, red). The thin anticyclonic band ($\zeta/f < 0$, blue) at the shoreline is consistent with surface currents vanishing at the nearshore boundary.

Bottom (b): The convergence band ($\delta/f < 0$, blue) collocated with the 15 m isobath is the bottom counterpart of the surface shear. Wave breaking and onshore Stokes drift drives onshore currents, compensated by offshore undertow near the bed; the red band of positive divergence ($\delta/f > 0$) just shoreward is consistent with the downward motion associated with the undertow return flow. Meanwhile, wave-induced bottom streaming, directed onshore in the direction of wave propagation, opposes the undertow near $h = 15\,\mathrm{m}$. Their meeting forces horizontal convergence, which by continuity drives upwelling, closing the loop back to the surface shear and vorticity generation above.

The right panel of Fig. 4 maps the ratio $\mathcal{R} = |\tau^{str}|/|r_D u_{\mathrm{bot}}|$ of wave streaming to bottom drag stress across the domain, following the quasi-linear scaling of McWilliams (2026) where $\mathcal{R} = A^2/\mu$, A being the wave slope and μ the current-to-phase-speed ratio. Offshore ($h > 100\,\mathrm{m}$), both streaming and drag are weak and $\mathcal{R} \ll 1$. On the inner shelf ($10 < h < 100\,\mathrm{m}$), $\mathcal{R}$ approaches and locally exceeds 1, confirming that streaming and drag genuinely compete there. The convergence zone visible in Fig. 4b sits precisely in this regime.

https://doi.org/10.5194/egusphere-2026-2942
Preprint. Discussion started: 17 July 2026

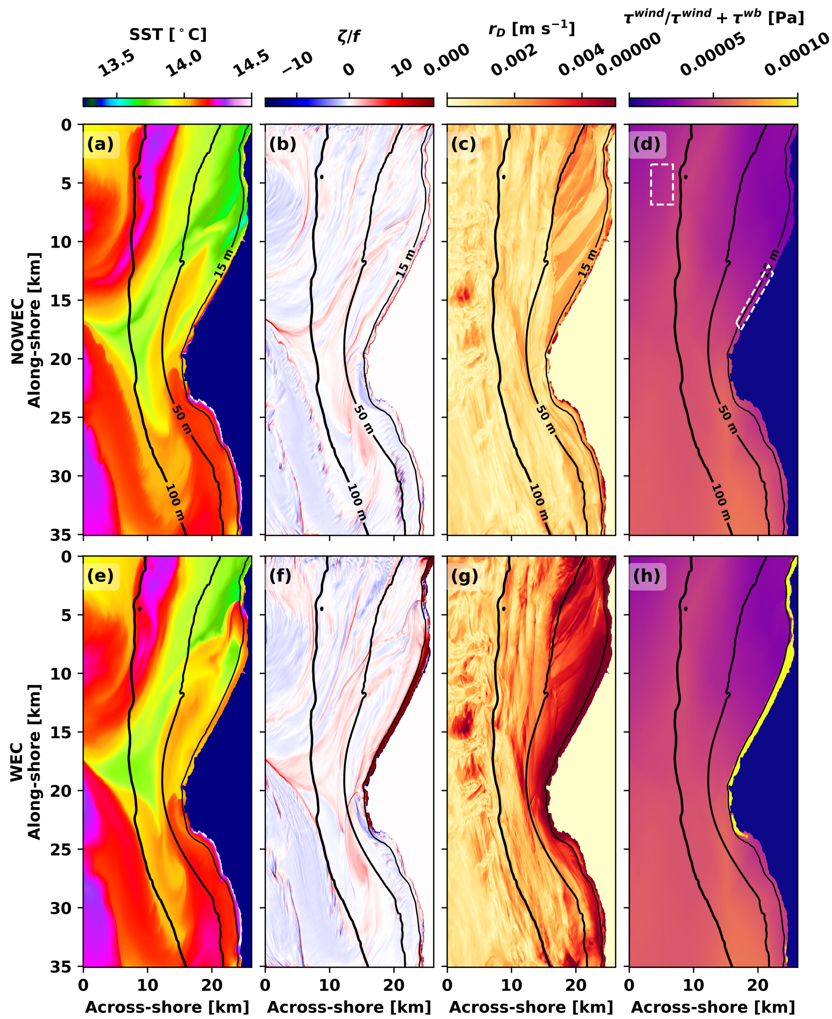

Figure 5. SST (a,e), normalized surface vorticity (b,f), drag coefficient (c,g) and surface stress (d,h) in configuration with (e-h) and without (a-d) wave effects on currents. Ocean time is 12/14/2006 (01:04:33 PCT). 15m, 50m and 100m isobaths (black). Offshore and nearshore domains used for spatial averaging in Fig. 6 and 7 (dashed white in panel d).

Fig. 5 compares spatial maps of SST, normalized surface vorticity, drag coefficient, and surface stress between the NOWEC and WEC configurations at the same time as panel (c) of Fig. 3 and Fig. 4, corresponding to the wave-breaking regime (14 Dec 2006, 14 days after initialization ensuring the solutions are spun up). At this particular time of low wind stress (d), the main features of the surface fields are largely similar between the two runs offshore, with submesoscale SST fronts (a, e) and vorticity structures (b, f) broadly consistent across configurations.

Nearshore, notable differences arise due to the incident NW swell with $H_s = 5.2$m. In the WEC run, the surface vorticity (f) exhibits enhanced positive vorticity concentrated along the coastline, while the NOWEC run is comparatively weak in

https://doi.org/10.5194/egusphere-2026-2942
Preprint. Discussion started: 17 July 2026

the same region. This nearshore vorticity enhancement is consistent with the spatial distribution of wave breaking: τ^{wind} is nearly identical[6] between the two runs offshore, while the addition of τ^{wb} in the WEC run produces a concentrated nearshore enhancement. The swell peak period T_p is long, around 15s here, yielding deep orbital velocity penetration. The bottom drag coefficient (g) is enhanced across a broader nearshore region than the breaking zone, extending wherever wave orbital velocities reach the seabed and amplify r_D.

Due to local geometry, the northern beaches are more exposed to the incident NW swell than the southern ones, resulting in stronger nearshore wave-current signatures in the north and relative sheltering in the south. These combined momentum effects produce a discernible imprint on SST: in the WEC run, wave-driven currents contribute to the northward advection of warm water along the coast (e), a signature that is weaker in the NOWEC run (a).

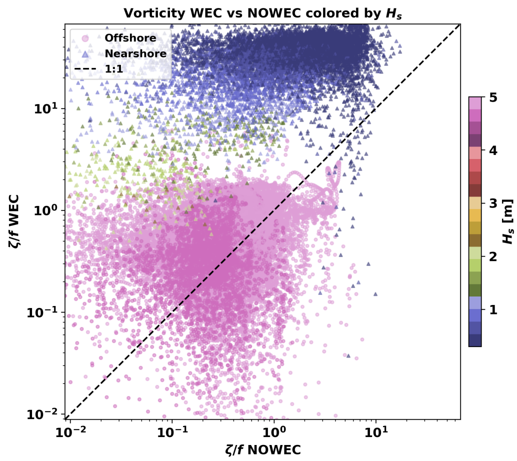

Figure 6. Scatter plot of normalized surface vorticity ζ/f (only cyclonic vorticity retained) from the WEC run against the NOWEC run, accumulating 5 hourly snapshots on 12/14/2006. Circles denote offshore grid points, triangles nearshore grid points (domains shown as dashed white in panel (d) of Fig. 5), and the dashed line is the 1:1 reference along which WEC has no effect on vorticity. Points above (below) the 1:1 line indicate WEC enhancement (reduction) of vorticity. Color indicates significant wave height H_s. Offshore, the distribution is broadly distributed above the 1:1 line, with 69% of points above the 1:1 line, reflecting a modest but systematic enhancement of cyclonic vorticity by WEC. Nearshore, the distribution is entirely shifted to positive values with a median enhancement factor of $\sim 20\times$, indicating that breaking wave momentum deposition systematically and strongly amplifies nearshore vorticity under "breaking" wave conditions ($H_s \lesssim 1$ m).

Fig. 6 quantifies the vorticity enhancement across both regimes. Offshore, the cloud is broadly distributed above the 1:1 line, with 69% of points above it, consistent with wave-enhanced frontogenesis intensifying submesoscale cyclonic vorticity (Hypolite et al., 2021). Nearshore, despite reduced wave amplitude due to breaking-induced dissipation and the nearshore tapering, momentum deposition by breaking drives vorticity enhancement an order of magnitude larger than in the NOWEC run (median enhancement factor of $\sim 20\times$), reflecting the generation and intensification of nearshore currents and topographic

[6] The wind stress computation uses a bulk formula with the relative wind (wind - currents) where currents are affected by waves with WEC.

https://doi.org/10.5194/egusphere-2026-2942
Preprint. Discussion started: 17 July 2026

wakes by τ^{wb} for this wave-breaking event. The contrast between the two distributions quantifies the fundamentally different role of WEC in the offshore and nearshore dynamical regimes, which we further analyze with a momentum balance below.

6.1.2 Nearshore versus offshore WEC horizontal momentum balance

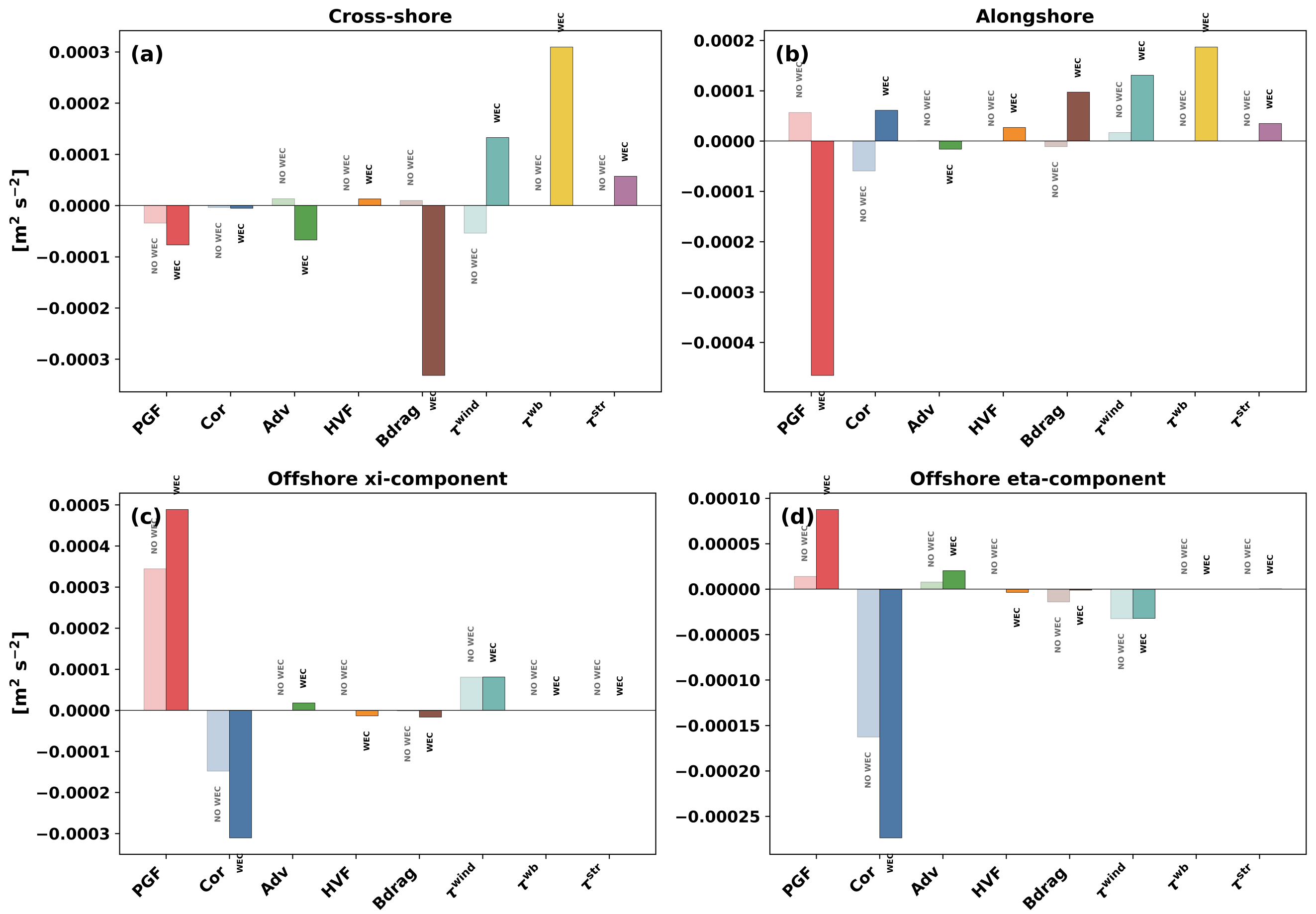

Figure 7. Spatially-averaged depth-integrated cross-shore (a) and alongshore (b) momentum tendencies [$m^2.s^{-2}$] in a nearshore subdomain and xi and eta components in an offshore subdomain (shown as dashed white in panel (d) of Fig. 5). Waves are coming from approximately 300° from north (northwest swell). Ocean time is 12/14/2006. Same colorcoding as in Fig. 2.

Fig. 7 shows the spatially-averaged depth-integrated momentum tendencies in the nearshore and offshore subdomains shown in Fig. 5, for both WEC and NOWEC configurations at the same snapshot time.

Offshore (Fig. 7 c-d), both WEC and NOWEC configurations exhibit a turbulent thermal wind balance between the pressure gradient force, wind and Coriolis, with advection as a secondary contribution. WEC slightly amplifies the amplitude of each term without altering the balance structure, consistent with the modest but systematic vorticity enhancement seen in Fig. 6.

https://doi.org/10.5194/egusphere-2026-2942
Preprint. Discussion started: 17 July 2026

The approximate symmetry between the xi and eta components of the offshore balance reflects the weak directional anisotropy of the offshore regime, away from the geometric constraint of the coastline. Breaking, streaming, and bottom drag are all negligible offshore. Specifically, breaking offshore is implicitly in the wind stress.

Nearshore (Fig. 7 a-b), the momentum balance is fundamentally different. The coastal boundary imposes a strong dynamical distinction between the cross-shore and alongshore directions. In the cross-shore direction, the NOWEC configuration is wind-driven, with wind stress balanced by bottom drag. The addition of WEC introduces depth-induced breaking stress as the dominant new term, compensated by a strongly enhanced bottom drag, shifting the balance from wind-versus-drag to breaking-plus-wind-versus-drag. Depth-induced breaking stress projects significantly onto the alongshore direction, driving currents in the direction of wave propagation (rather than purely cross-shore or opposing it). The pressure gradient force adjusts to accommodate the extra wave-induced forcing, while the NOWEC configuration retains a turbulent thermal wind balance between Coriolis, PGF, and wind. This wave-driven setup of a large pressure gradient force produces strong alongshore currents, consistent with the SST signature visible in Fig. 6.

This nearshore balance is very consistent with the surfzone balance of Duck94 identifying PGF, drag and breaking as the dominant momentum terms in balance. The main differences arise from the coastal morphology, with Duck being an alongshore uniform barred beach and the region of Pt. Arguello being an unbarred, morphologically complex coast, driving PGF in both the cross-shore and alongshore directions.

6.2 Towards surf-resolving wave forcing

The nearshore tapering scheme introduced in Sec. 6.1 is a pragmatic response to two compounding limitations: a resolution mismatch between the wave and ocean components of the coupled ROMS-NCWEC-WW3 system, and the fact that neither grid is fine enough to resolve depth-induced breaking. Physically, the tapering reproduces what depth-induced breaking would naturally produce at sufficient resolution: a progressive decay of wave amplitude toward the shoreline. In the present configuration, WW3 is run at coarser resolution (300 m) than the 30 m ocean grid and reinterpolated onto it, so the shoaling and breaking gradient of the surfzone is never resolved in the wave field to begin with. Even a 30 m WW3 configuration would remain insufficient, since naturally resolving depth-induced breaking requires $\mathcal{O}(1\text{–}5)$ m wave model resolution, placing the problem in the KPP grey zone for turbulence closure (Wyngaard, 2004).

Several avenues exist toward removing the wave-side limitation. A first option is to run WW3 on an unstructured grid with higher resolution nearshore, which would allow depth-induced breaking to be represented at the ocean grid scale without reinterpolation.

A second option is to use a parent-grid WW3 solution and prescribe one or several spectrum-peak waves at the offshore domain boundary and transport them inward using the inline WKB solver (see Appendix B), which resolves the wave field on the ocean grid by construction and remains consistent with the resolved bathymetry and currents. This approach is attractive in that it requires offshore spectral information only.

A third, more speculative avenue is offered by emerging parametric wave models such as PiCLES (Hell et al., 2025). Instead of solving the spectral action balance on an Eulerian grid, as WW3 does, PiCLES tracks a sparse ensemble of Lagrangian wave

https://doi.org/10.5194/egusphere-2026-2942
Preprint. Discussion started: 17 July 2026

particles. The computational cost is reduced by one order of magnitude in idealized wind-sea cases, while significant wave height and Stokes drift diagnostics are broadly consistent with WW3. Because wave information is carried on particles rather than on a fixed spectral grid, this framework can in principle provide wave forcing at arbitrary ocean-model resolution.

All three avenues address only the wave-side limitation. Surf-resolving the ocean grid places the model in the KPP grey zone and, at fixed computing resources, forces a domain reduction that would sacrifice the regional submesoscale circulation this configuration is designed to resolve. Coupled systems such as ROMS/COAWST (Kumar et al., 2012) typically address this tension through telescoping nested grids that refine into the surfzone while preserving a regional parent domain. This strategy enables explicit representation of surfzone dynamics but pushes the surfzone in the grey zone. The grey zone is handled through GLS-family closures such as k-ϵ, which Chen et al. (2025) show produce accurate mean-state profiles but over-damp resolved turbulence. Independently, elevated horizontal viscosity is required for numerical stability at high resolution and across grid transitions, further damping resolved dynamics in ways that are neither physically justified nor measured. The present ROMS-NCWEC configuration represents the complementary compromise, retaining regional submesoscale dynamics and non-conservative wave effects with no additional horizontal viscosity ($\nu_h = 0$), at the cost of a tapered surfzone.

7 Conclusions

We present ROMS-NCWEC, an updated and extended implementation of non-conservative wave effects on currents in ROMS, one-way coupled to WaveWatch3 to resolve a broadband wave field. Three non-conservative effects are described: wave breaking, wave-induced bottom streaming, and wave-enhanced bottom drag. Each can be represented as a boundary stress or as a 3D body force, with wave-enhanced eddy viscosity and diffusivity parameterized following Romero et al. (2021) to account for whitecapping. The implementation is validated against the Duck 1994 experiment, using either an offline wave forcing file or the inline WKB solver, recovering the essential nearshore flow features including the surf-zone overturning circulation and alongshore jet, with normalized RMS errors within the range of previous studies (but using only 20 comparison points against 42) with no explicit horizontal diffusion. The implementation also introduces a modified bottom boundary layer thickness criterion accounting for wave streaming, and improves temporal consistency by recomputing WEC forces and KPP mixing at the corrector stage of the predictor-corrector time stepping scheme.

The regional application to Pt. Arguello represents the first realistic ROMS-NCWEC application including breaking momentum at a resolution that does not resolve the surfzone. Prior realistic implementations of breaking momentum in ROMS and COAWST (Uchiyama et al., 2010; Kumar et al., 2012; Wu et al., 2021) were all designed to explicitly resolve the surfzone, with the finest grids reaching $dx = 8$m resolution. Operating at 30m resolution in a surfzone-permitting rather than surfzone-resolving regime with WW3 forcing at coarser resolution requires the nearshore tapering scheme introduced in Sec. 5.1, which regularizes unbounded wave quantities while parameterizing the bulk effect of unresolved depth-induced breaking in an uncalibrated but internally consistent way.

In this framework, the regional momentum balance reveals dynamically distinct offshore and nearshore behaviors. Offshore, swells through WEC slightly amplify the terms in the turbulent thermal wind balance while preserving it as the governing

https://doi.org/10.5194/egusphere-2026-2942
Preprint. Discussion started: 17 July 2026

balance, consistent with wave-enhanced frontogenesis intensifying submesoscale cyclonic vorticity. Nearshore, breaking stress emerges as the dominant WEC addition, producing vorticity enhancements of order $20\times$ relative to the no-wave control run and shifting the momentum balance from wind-versus-drag to breaking-plus-wind-versus-drag. The streaming-to-drag ratio provides a first spatial assessment of their competition in a realistic regional model: streaming matters on the inner shelf ($10\,\mathrm{m} < h < 100\,\mathrm{m}$), where wave bottom boundary layer thickness is sufficient for streaming to genuinely compete with enhanced drag, while interpretation in the breaking zone remains complicated by the nonlinear dependence of τ^{cd} on wave amplitude through the Soulsby parameterization. Despite the uncalibrated nature of the nearshore tapering, the model produces a physically consistent dynamical picture: wave breaking drives strongly sheared alongshore jets at the surface, while near-bed convergence between wave-induced streaming and the undertow return current drives upwelling, closing a wave-forced overturning cell.

Together, these results establish ROMS-NCWEC as a viable framework for inner-shelf-resolving, surfzone-permitting regional ocean modeling with non-conservative wave effects. This intermediate-resolution regime, fine enough to permit nearshore dynamics and retain regional submesoscale currents, yet coarser than the surfzone, opens a new avenue for exploring the interaction between breaking-driven nearshore circulation, wave streaming, and submesoscale processes along complex coastlines, a class of problems that neither surfzone-resolving nor coarse regional models have been able to address.

Ideally, future models will resolve all necessary scales simultaneously. Several avenues exist toward this goal: the nearshore tapering could be avoided by using WW3 on an unstructured grid with higher resolution nearshore; WW3 wave spectra prescribed at the domain boundary could be transported inward via the inline WKB solver; alternatively, emerging parametric wave models such as PiCLES (Hell et al., 2025) offer a computationally efficient Lagrangian framework that could provide wave forcing at the ocean model resolution, potentially circumventing the resolution mismatch that motivates the present nearshore tapering scheme, though current implementations remain limited to deep-water wind-sea and do not yet provide the nearshore dissipation rates required by ROMS-NCWEC.

Code and data availability. The ROMS-NCWEC model code (v1.0.0) is archived on Zenodo at https://doi.org/10.5281/zenodo.20498888 (Hypolite et al., 2026a). The Pt. Arguello simulation input files (grid, boundary, initial condition, and WW3 wave forcing) are archived at https://doi.org/10.5281/zenodo.20499100 (Hypolite et al., 2026b). The Duck 1994 experiment benchmark simulation is reproducible using the code at https://doi.org/10.5281/zenodo.21384107 (Hypolite et al., 2026c) including the grid, the wave forcing file and the configuration file. The current meter time series are archived at https://doi.org/10.5281/zenodo.8286253.

https://doi.org/10.5194/egusphere-2026-2942
Preprint. Discussion started: 17 July 2026

Appendix A: ROMS-NCWEC compilation options tree

ROMS-NCWEC is controlled through a set of C preprocessor (CPP) compilation options, preprocessor directives applied to the Fortran source files prior to compilation, that select which wave effects are active, how wave forcing is provided, and how each non-conservative process is represented. The options are organized hierarchically: a master WEC flag guards all wave-related modules, wave forcing is selected among offline (`WAVE_OFFLINE`), inline WKB (`WKB_WWAVE`, see appendix B), or analytical (`ANA_WEC_FRC`) sources, and each non-conservative effect, breaking, streaming, and bottom drag, has dedicated flags controlling its momentum representation (surface stress or 3D body force) and its mixing parameterization. Several debug flags allow individual terms to be zeroed for sensitivity testing. Table A1 provides representative examples of compilation option combinations for common use cases, and a simplified option tree is illustrated in Fig. A1.

ROMS-NCWEC CPP options:

- `WEC` guards all WEC-related modules in the code.

- `MONOWAVE` uses the mean-peak monochromatic expressions for Stokes drift, setup, and dissipation. Applicable with any wave source (`WKB_WWAVE`, `WAVE_OFFLINE`, or `ANA_WEC_FRC`). If undefined, the code uses the broadband (spectral) approximation, which requires additional fields (see Sec. 2.2.2) from a spectral model and therefore must be used jointly with `WAVE_OFFLINE`.

- `WAVE_OFFLINE` reads wave fields from a NetCDF input file (WW3 format). Alternative to `WKB_WWAVE` and `ANA_WEC_FRC`. Provides $a, T, \theta, \varepsilon^{wb}, \varepsilon^{str}$ from file.

- `UORBOFF` reads the orbital velocity from the WW3 input file. Requires `WAVE_OFFLINE`. If undefined, orbital velocity is computed internally using the mean-peak monochromatic expression.

- `SUP_OFF` reads the wave set-down from the WW3 input file (sign convention $\hat{\eta} < 0$). Requires `WAVE_OFFLINE`. If undefined, setup is computed internally using the mean-peak monochromatic expression.

- `WKB_WWAVE` turns on the inline WKB wave model. Alternative to `WAVE_OFFLINE` and `ANA_WEC_FRC`. Guards all WKB-related modules. Given offshore boundary conditions set in `wkb_wwave.opt` (see table H1), the WKB solver propagates wave action and wavenumber on the ROMS grid, producing a wave field consistent with the bathymetry (shoaling, refraction, breaking saturation) and optionally the currents (`WKB_CEW`). The WKB model is inherently monochromatic (single peak frequency and direction). Must have `MONOWAVE` defined.

- `WKB_STEADY` before the main simulation, iterates the WKB solver to steady state (up to 100 000 iterations): advances the wave action and wavenumber equations with no current feedback until convergence. This produces a self-consistent initial wave field that satisfies the action balance with all dissipation terms active, avoiding transient wave adjustment in the first time steps.

https://doi.org/10.5194/egusphere-2026-2942
Preprint. Discussion started: 17 July 2026

- WKB_FRC_BRY maintains wave action and wavenumber at open boundaries from prescribed offshore conditions (allocated per active OBC_⋆ side). Required when the WKB domain has open boundaries.

- WKB_CEW enables current effects on waves in the WKB solver (two-way coupling). When defined, the group velocity includes the depth-averaged current, refraction includes current shear terms, and the dispersion relation uses the time-varying free surface instead of a static tide level.

- BREAK_TG83 WKB sub-option. Computes the breaking dissipation ε^{wb} following Thornton & Guza (1983): ensemble-averaged bore dissipation integrated over the Rayleigh wave-height distribution weighted by a breaking-probability function. User must choose exactly one of BREAK_TG83, BREAK_TG83A, or BREAK_CT93.

- BREAK_TG83A WKB sub-option. Computes the breaking dissipation ε^{wb}. Modified form of BREAK_TG83 with improved treatment of the breaking probability.

- BREAK_CT93 WKB sub-option. Computes the breaking dissipation ε^{wb} following Church & Thornton (1993). Replaces the monomial $H_\star^7$ dependence in BREAK_TG83/BREAK_TG83A with two smooth shape functions, producing a more robust and physically realistic parameterization.

- ANA_WEC_FRC alternative to WKB_WWAVE and WAVE_OFFLINE. User hardcodes the wave variables $(a, T, \theta, \varepsilon^{wb}, \varepsilon^{str})$ that are otherwise filled by WKB_WWAVE or WAVE_OFFLINE. Useful for sanity checks, e.g., prescribing a uniform wave field or an exact analytical solution to verify the WEC machinery in isolation. Must have MONOWAVE defined.

- BREAKING master switch for breaking momentum forcing. Without this, no breaking effects at all.

- SURFACE_BREAK sub-flag of BREAKING. Enables breaking momentum forcing on currents. Without it, breaking is still computed (e.g. for wave-enhanced mixing K_v^{wb})but no momentum is applied. By default (without BODY_BREAK), breaking is applied as a surface stress added to the wind stress.

- BODY_BREAK sub-flag of SURFACE_BREAK. Controls the form of momentum application: When both SURFACE_BREAK and BODY_BREAK are defined, breaking is instead distributed as a 3D body force with a vertical profile function. When SURFACE_BREAK is defined but BODY_BREAK is undefined, breaking remains a surface stress.

- Akb_U2010: selector within the K_v^{wb} computation (requires BREAKING && LMD_MIXING && !AKB0). When defined, computes K_v^{wb} following U2010, Eq. (31) (monochromatic, C_b-based). When undefined, uses the Romero et al. (2021) breaking viscosity.

- AKB0: Debug flag sub-flag of BREAKING: Zeros out the breaking-induced eddy viscosity K_v^{wb} when defined.

- BRK0 Debug flag sub-flag of BREAKING: Zeros out the breaking dissipation rate when defined. Disables all breaking momentum forcing.

https://doi.org/10.5194/egusphere-2026-2942
Preprint. Discussion started: 17 July 2026

- `WAVE_FRICTION` enables bottom wave-friction dissipation. The friction dissipation rate is computed (WKB), imposed (`ANA_WEC_FRC`) or read from file (`WAVE_OFFLINE`) and applied to the momentum equations.
- `BODY_FRICTION` when defined alongside `WAVE_FRICTION`, distributes the bottom streaming as a 3D body force with a vertical profile function, rather than applying it only at the bottom layer.
- `FRC0`: sub-flag of `WAVE_FRICTION`. When defined, zeros out the streaming momentum frc(i,j) = 0. The friction dissipation is still computed, but its momentum forcing on currents is suppressed. Diagnostic use: isolate the effect of bottom streaming on the circulation.
- `FRC_HBBL0`: sub-flag of `WAVE_FRICTION`. When defined, removes the streaming contribution to bottom boundary layer (BBL) depth detection in `lmd_kpp.F`. Without it, streaming adds a term to Cr (the bulk Richardson number criterion) that deepens the detected BBL. Diagnostic use: test KPP sensitivity to streaming-enhanced BBL.
- `BBL_S95` enables wave-enhanced bottom drag following Soulsby (1995). Uses the wave orbital velocity at the bed to augment the combined wave-current bottom stress.
- `WMB0`: sub-flag of `BBL_S95`. When defined, disables wave-enhanced bottom mixing in the KPP bottom boundary layer scheme (BKPP). Without it, the wave-current drag coefficient `r_D` (from Soulsby 1995) enhances the near-bed turbulent mixing velocity scale. Diagnostic use: isolate wave-enhanced bottom drag from wave-enhanced bottom mixing.
- `SURFACE_ROLLER` enables surface roller dynamics following U2010 (see §B4 in Appendix B). The roller stores energy from breaking and releases it shoreward with a delay, providing a more realistic cross-shore distribution of breaking forces in the surf zone.
- `WAVE_RAMP` gradually spins up wave forcing during cold starts. The ramp factor $r = \tanh(48\,\Delta t\,(i_{\rm ic} - n_{\rm tstart})/86400)$ multiplies wave height linearly and dissipation quadratically (r^2). Reaches $\sim$96% strength in $\sim$1 hour (for $\Delta t = 3$ s). Prevents a quiescent ocean from being hit with full wave forcing instantaneously, avoiding numerical blowup at step 1.
- `KPPLT` KPP Langmuir Turbulence parameterization (P. Wang, personal communication, 2021; implemented in Hypolite et al. 2023). Enhances KPP turbulent velocity scales w_m, w_s by a factor depending on the turbulent Langmuir number $La = \sqrt{u_*/|\mathbf{u}^{\rm St}|}$ and wind-Stokes alignment. Requires `WEC` and `LMD_KPP`. Recommended usage only for grid resolution coarser than 300m, otherwise risk of double counting vertical displacement with partial resolution of Langmuir circulations.
- `DIAGNOSTICS` enables online momentum-balance diagnostics computation (not WEC-specific, but records WEC forcing terms when `WEC` is active).

https://doi.org/10.5194/egusphere-2026-2942
Preprint. Discussion started: 17 July 2026

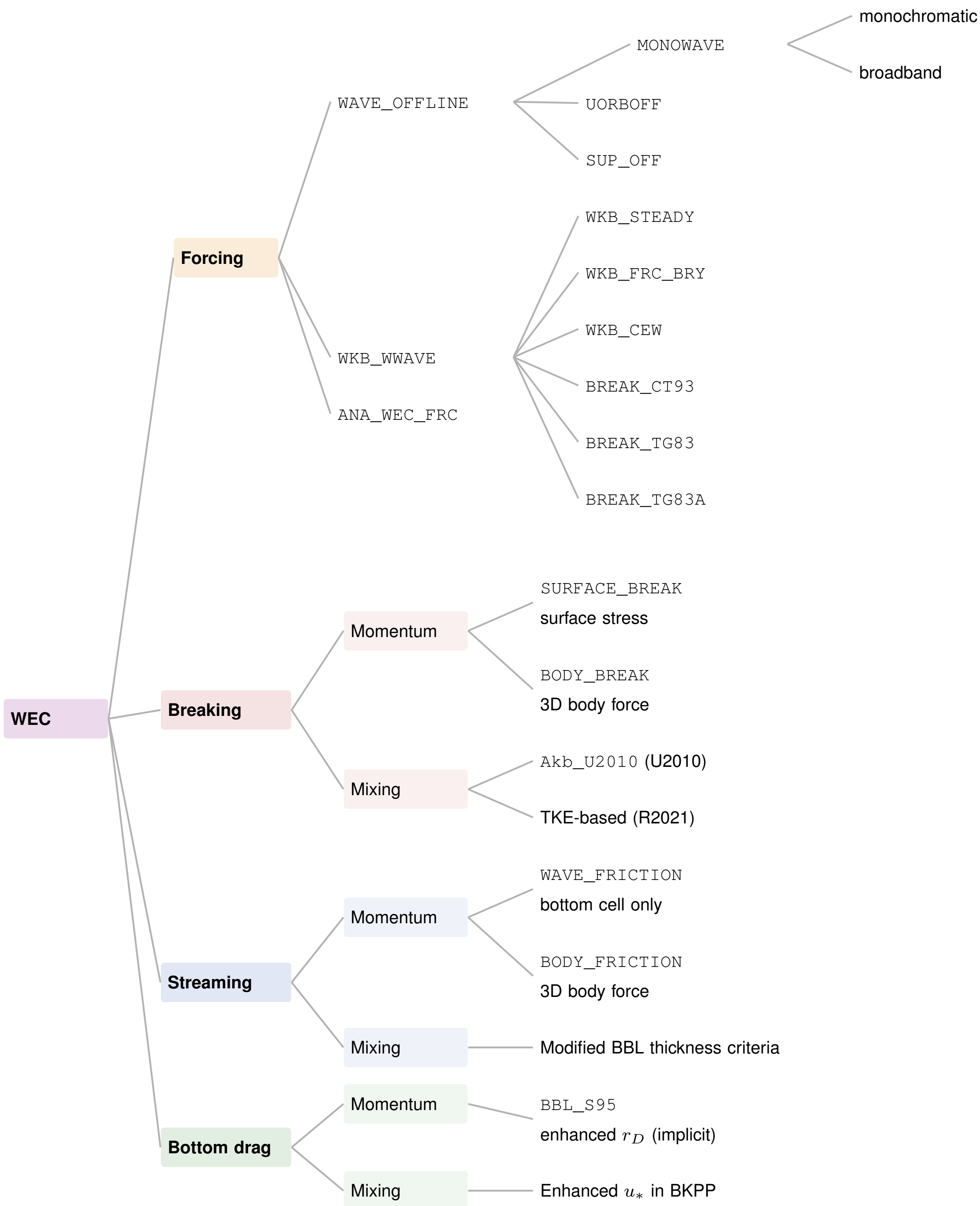

Figure A1. Compilation options tree for the ROMS-NCWEC framework. The tree illustrates the available CPP preprocessing flags organized by wave effect category: forcing source, wave breaking, wave streaming, and wave-enhanced bottom drag.

https://doi.org/10.5194/egusphere-2026-2942
Preprint. Discussion started: 17 July 2026

Table A1. Examples of runs and their non-conservative WEC compilation options.

	Breaking					Streaming				Bottom drag		Comments
	SURFACE_BREAK	BODY_BREAK	BRK0	AKB0	Akb_U2010	WAVE_FRICTION	BODY_FRICTION	FRC0	FRC_HBBL0	BBL_S95	WMB0	
	✗	✗	✓	✓	✗	✗	✗	✗	✓	✗	✓	No NC
	✓	✗	✗	✗	✗	✓	✗	✗	✗	✓	✗	All realistic NC
	✓	✗	✗	✗	✗	✓	✗	✗	✓	✓	✗	Isolate friction in HBBL
	✓	✗	✗	✗	✗	✓	✗	✗	✗	✓	✓	Isolate friction in HBBL mixing
	✓	✓	✗	✗	✗	✓	✓	✗	✗	✓	✗	Using body forces
6	✓	✗	✓	✗	✗	✓	✗	✗	✗	✓	✗	Disabling momentum via breaking
	✓	✗	✗	✓	✗	✓	✗	✗	✗	✓	✗	Disabling mixing via breaking
	✓	✗	✗	✗	✓	✓	✗	✗	✗	✓	✗	Testing monochromatic mixing via breaking
	✗	✗	✓	✓	✗	✗	✗	✗	✓	✓	✗	Isolate bottom drag
	✗	✗	✓	✓	✗	✓	✗	✗	✗	✗	✓	Isolate streaming
	✗	✗	✓	✓	✗	✓	✗	✓	✗	✗	✓	Isolate streaming momentum

Appendix B: Spectrum-peak wave model in ROMS-NCWEC

The WKB wave model in UCLA-ROMS solves three coupled conservation equations on the ROMS grid at the barotropic time step Δt_{fast}. It provides a self-contained, inline alternative to reading pre-computed wave fields (`WAVE_OFFLINE`). The model assumes monochromatic, slowly-varying (WKB) waves, and computes:

1. Wavenumber vector $\mathbf{k} = (k_\xi, k_\eta)$, ray equations (wave refraction by depth and currents).
2. Wave action density $\mathscr{A}$, energy budget (propagation, breaking, friction).
3. Surface roller action $\mathscr{A}^r$, delayed momentum transfer from breaking (`#ifdef SURFACE_ROLLER`).

B1 Group velocity

The group velocity magnitude is:

$$c_g = n\,c = \frac{\sigma}{k}\,n, \qquad n = \frac{1}{2}\left(1 + \frac{2kD}{\sinh 2kD}\right), \tag{B1}$$

where $c = \sigma/k$ is the phase speed. In the presence of a mean current $\bar{\mathbf{u}}$, the group velocity vector is (U2010, Eq. 17):

$$\mathbf{c}_g = \bar{\mathbf{u}} + \frac{c_g}{k}\mathbf{k}, \tag{B2}$$

https://doi.org/10.5194/egusphere-2026-2942
Preprint. Discussion started: 17 July 2026

and the phase velocity vector (used for roller advection) is:

$$\mathbf{c} = \bar{\mathbf{u}} + \frac{c}{k}\,\mathbf{k} = \bar{\mathbf{u}} + \frac{\sigma}{k^2}\,\mathbf{k}. \tag{B3}$$

The code stores c_g/k in `wcg` and c/k in `wcr`, so that the velocity components are recovered via multiplication by (k_ξ, k_η).

Without currents (`#ifndef WKB_CEW`), the $\bar{\mathbf{u}}$ terms are omitted.

B2 Wavenumber refraction

The wavenumber vector $\mathbf{k} = (k_\xi, k_\eta)$ evolves along rays according to (U2010, Eq. 14):

$$\frac{\partial \mathbf{k}}{\partial t} + \mathbf{c}_g \cdot \nabla \mathbf{k} = -\frac{k\,\sigma}{\sinh 2kD}\,\nabla D \qquad \underbrace{-\tilde{\mathbf{k}} \cdot \nabla \bar{\mathbf{u}}}_{\text{current refraction (WKB\_CEW)}} \quad . \tag{B4}$$

In component form with curvilinear metric terms $p_m = 1/\Delta\xi$, $p_n = 1/\Delta\eta$:

$$\frac{\partial k_\xi}{\partial t} + c_{g,\xi}\,p_m\,\frac{\partial k_\xi}{\partial \xi} + c_{g,\eta}\,p_n\,\frac{\partial k_\xi}{\partial \eta} = -c_0\,p_m\,\frac{\partial D}{\partial \xi} - k_\xi\,p_m\,\frac{\partial \bar{u}}{\partial \xi} - k_\eta\,\overline{\left(\frac{\partial \bar{v}}{\partial \xi}\right)}_\psi, \tag{B5}$$

$$\frac{\partial k_\eta}{\partial t} + c_{g,\xi}\,p_m\,\frac{\partial k_\eta}{\partial \xi} + c_{g,\eta}\,p_n\,\frac{\partial k_\eta}{\partial \eta} = -c_0\,p_n\,\frac{\partial D}{\partial \eta} - k_\eta\,p_n\,\frac{\partial \bar{v}}{\partial \eta} - k_\xi\,\overline{\left(\frac{\partial \bar{u}}{\partial \eta}\right)}_\psi, \tag{B6}$$

where:

$$c_0 \equiv \frac{\sigma\,k}{\sinh 2kD} \tag{B7}$$

is the depth-refraction coefficient (vanishes in deep water), and the ψ-point average denotes interpolation of current gradients from staggered u/v-points to psi-points (4-point average in the code).

The current refraction terms are only active with `#ifdef WKB_CEW`.

B3 Wave action conservation

The specific wave action $\mathscr{A} = E/(\rho_0\,\sigma) = g\,H_{\mathrm{rms}}^2/(8\sigma)$ satisfies (U2010, Eq. 15):

$$\frac{\partial \mathscr{A}}{\partial t} + \nabla \cdot (\mathscr{A}\,\mathbf{c}_g) = -S_b - S_d, \tag{B8}$$

where $S_b = \varepsilon^{wb}/(\rho_0\sigma)$ is the breaking sink and $S_d = \varepsilon^{str}/(\rho_0\sigma)$ is the friction sink (both in action units).

The divergence is expanded as:

$$\nabla \cdot (\mathscr{A}\,\mathbf{c}_g) = \mathbf{c}_g \cdot \nabla \mathscr{A} + \mathscr{A}\,\nabla \cdot \mathbf{c}_g, \tag{B9}$$

where $\mathbf{c}_g \cdot \nabla \mathscr{A}$ is advection and $\mathscr{A}\,\nabla \cdot \mathbf{c}_g$ accounts for shoaling (convergence of group velocity amplifies wave action) and current divergence (with `WKB_CEW`).

https://doi.org/10.5194/egusphere-2026-2942
Preprint. Discussion started: 17 July 2026

B3.1 Surface roller action equation (`#ifdef SURFACE_ROLLER`)

When a wave breaks, a fraction α_r of the breaking energy feeds the surface roller, a turbulent mass of water carried forward on the wave face at the phase velocity $\mathbf{c}$. The roller action $\mathscr{A}^r = E^r/(\rho_0\sigma)$ satisfies (U2010, Eq. 40):

$$\frac{\partial \mathscr{A}^r}{\partial t} + \nabla\cdot(\mathscr{A}^r\,\mathbf{c}) = \frac{\alpha_r\,\varepsilon^{wb} - \varepsilon^r}{\rho_0\,\sigma} = \alpha_r\,S_b - S_r. \tag{B10}$$

A key difference when comparing to the wave action equation is that the roller propagates at phase velocity $\mathbf{c}$ (faster than $\mathbf{c}_g$), shifting momentum input shoreward. The fraction of breaking energy entering the roller is a source term. Note that the roller has its own dissipation rate $-S_r$.

Without `SURFACE_ROLLER`, $\alpha_r = 0$ (no roller):[7] all breaking energy directly forces currents, $S_b\,\sigma = \varepsilon^{wb}/\rho_0$. When $\alpha_r = 1$ (full roller, typical): primary breaking produces no direct momentum forcing; instead, all energy enters the roller and only the roller dissipation ε^r drives currents. This shifts the forcing shoreward (roller propagates at $c > c_g$). When $0 < \alpha_r < 1$: a fraction $(1-\alpha_r)$ of breaking acts immediately; the rest is delayed through the roller.

Roller dynamics should be used in surfzone-resolving configurations where $dx \ll L_r \approx D/\sin\beta \approx 10\,D$. Since L_r vanishes with depth nearshore, the roller is self-limiting and always dissipates within the surfzone. On coarser grids where $L_r < dx$, the roller dissipates within the same cell where it is generated, producing no spatial redistribution of momentum. The roller equation reduces to an unnecessary intermediary and deactivating `SURFACE_ROLLER` gives equivalent results at lower cost.

B3.2 Dissipation parameterizations

Depth-induced breaking: The primary breaking parameterization is Church and Thornton (1993), which extends Thornton and Guza (1983) by adding a smooth onset switch (U2010, Eq. 39):

$$\varepsilon^{wb} = \frac{3\sqrt{\pi}}{16}\,\rho_0\,g\,\frac{B_b^3\,f_p}{D}\,H_{\rm rms}^3\;\underbrace{\left[1+\tanh\left(8\left(\frac{H_{\rm rms}}{\gamma_b D}-1\right)\right)\right]}_{F_{\rm tanh}:\ \text{onset switch}}\;\underbrace{\left[1-\left(1+\left(\frac{H_{\rm rms}}{\gamma_b D}\right)^2\right)^{-5/2}\right]}_{F_{\rm prob}:\ \text{breaking fraction}}, \tag{B11}$$

where $f_p = \sigma/(2\pi)$ is the peak frequency.

The breaking dissipation in action units (the actual sink in Eq. B8) is:

$$S_b = \frac{\varepsilon^{wb}}{\rho_0\,\sigma}\,. \tag{B12}$$

Two alternative breaking formulations are also available:

CPP flag	Formula	Reference
`BREAK_TG83`	$\varepsilon^{wb} \propto H^7/(\gamma_b^4 D^5)$	Thornton and Guza (1983)
`BREAK_TG83A`	$\varepsilon^{wb} \propto H^5/(\gamma_b^2 D^3) \times F_{\rm prob}$	Thornton and Guza (1983)
`BREAK_CT93`	Eq. (B11)	Church and Thornton (1993)

[7] In the code the full branch `SURFACE_ROLLER` is deactivated, not merely α_r set to 0.

https://doi.org/10.5194/egusphere-2026-2942
Preprint. Discussion started: 17 July 2026

Roller dissipation: The roller dissipates by shear at its front face (U2010, Eq. 41):

$$\varepsilon^r = \frac{g \sin\beta\, E^r}{c} = g \sin\beta\, \rho_0\, \mathscr{A}^r\, \frac{\sigma}{c} = g \sin\beta\, \rho_0\, \mathscr{A}^r\, k, \tag{B13}$$

using $\sigma/c = k$. In action units:

$$S_r = \frac{\varepsilon^r}{\rho_0\, \sigma} = g \sin\beta\, \mathscr{A}^r\, \frac{k}{\sigma}. \tag{B14}$$

Bottom wave friction: Rayleigh-averaged friction dissipation (U2010, Eq. 36):

$$\varepsilon^{str} = \frac{1}{2\sqrt{\pi}}\, \rho_0\, f_w\, |u^w_{\mathrm{orb}}|^3. \tag{B15}$$

using Soulsby (1995) wave friction factor f_w. In action units:

$$S_d = \frac{\varepsilon^{str}}{\rho_0\, \sigma} = \frac{1}{2\sqrt{\pi}}\, \frac{f_w}{\sigma}\, |u^w_{\mathrm{orb}}|^3. \tag{B16}$$

B4 Transfer to WEC: Dissipation and Stokes Drift

B4.1 Breaking force: Combined ε_b and ε_r

The momentum forcing from breaking uses the total effective dissipation (U2010, Eq. 48, 50):

$$\frac{\varepsilon_{\mathrm{tot}}}{\rho_0} = \frac{(1-\alpha_r)\,\varepsilon^{wb} + \varepsilon^r}{\rho_0} = \left[(1-\alpha_r)\, S_b + S_r\right] \sigma. \tag{B17}$$

B4.2 Friction dissipation

$$\texttt{wved(i,j)} = S_d\, \sigma = \frac{\varepsilon^{str}}{\rho_0}. \tag{B18}$$

B4.3 Wave Direction

$$\texttt{wdrx} = \frac{k_\xi}{k}, \qquad \texttt{wdre} = \frac{k_\eta}{k}. \tag{B19}$$

B4.4 Stokes Drift with Roller Contribution

The total Stokes transport includes both wave action and roller action (U2010, Eq. 43):

$$\mathbf{U}^{\mathrm{St}} = \frac{(\mathscr{A} + \mathscr{A}^r)\,\sigma}{\rho_0}\, \mathbf{k} = \frac{E + E^r}{\rho_0\, \sigma}\, \sigma\, \mathbf{k} = \frac{(E + E^r)}{\rho_0}\, \frac{\mathbf{k}}{1}. \tag{B20}$$

The Stokes action used for the monochromatic (`MONOWAVE`) Stokes drift profile is:

$$\texttt{act(i,j)} = R^2 \left[\frac{1}{\sigma}\, \frac{g\, H_{\mathrm{rms}}^2}{8} + \mathscr{A}^r \right] = R^2 \left[\mathscr{A} + \mathscr{A}^r \right], \tag{B21}$$

where $R = R(t)$ is the wave ramp (see `WAVE_RAMP`). Without `SURFACE_ROLLER`, the roller term is absent.

The 3D Stokes velocity profile (U2010, Eq. 44) uses the exponential monochromatic formula:

$$\mathbf{u}^{\mathrm{St}}(z) = \frac{\sigma^2 \cosh[2k(z+h)]}{g \sinh^2(kD)}\, (\mathscr{A} + \mathscr{A}^r)\, \mathbf{k}. \tag{B22}$$

https://doi.org/10.5194/egusphere-2026-2942
Preprint. Discussion started: 17 July 2026

Appendix C: Symbol definitions

Symbol	Description
Coordinates	
x, y	Horizontal Cartesian coordinates which we denote $\perp$
z	Vertical Cartesian coordinate
$\hat{z}$	Vertical unit vector
xi (ξ), eta (η)	Horizontal curvilinear ROMS coordinates analog of (x, y)
sigma-level	Terrain-following vertical ROMS coordinate (NB: different than intrinsic radial frequency σ)
ρ-points	Cell centers, where tracers (temperature, salinity, density) and free surface live
u-points	Midpoints of the western/eastern cell faces, where the xi-component of velocity (u) lives
v-points	Midpoints of the southern/northern cell faces, where the eta-component of velocity (v) lives
ψ-points	Cell corners, offset by half a grid cell in both xi and eta from ρ

Table D1. Variable definitions.

https://doi.org/10.5194/egusphere-2026-2942
Preprint. Discussion started: 17 July 2026

Symbol	Description
Variables (not wave-related)	
$\mathbf{u}, w$	Eulerian 3D velocity field [m.s^{-1}]
ζ	Vorticity [m.s^{-2}]
t	Ocean time [s]
ϕ	Potential function [s^{-2}]
$\mathbf{F}$	Non-conservative forces [m.s^{-2}]
$\mathbf{D}$	Current-only vertical mixing force [m.s^{-2}]
ρ	Water density anomaly [kg.m^{-3}]
η	Sea surface height [m] (Sec. 1-6) / curvilinear coordinate (Appendix B)
c	Tracer concentration [units depend on tracer]
$\mathscr{C}$	Non-conservative tracer forcing [units of c times s^{-1}]
K_v	Turbulent eddy viscosity [m^2.s^{-1}]
K_v^{cd}	Turbulent eddy viscosity from current [m^2.s^{-1}]
$\mathcal{D}_\perp$	Hyperdiffusion term [m.s^{-2}]
τ^{wind}	Wind stress [m^2.s^{-2}]
τ^{cd}	Bottom drag stress [m^2.s^{-2}]
τ_c	Bottom drag stress due to current (in Eq. 38-39) [m^2.s^{-2}]
r_D	Bottom drag coefficient [m.s^{-1}]
u_{bot}	Bottom velocity $= u\vert_{-h}$ [m.s^{-1}]
h_{BBL}	Bottom boundary layer thickness [m]
N^2	Stratification [s^{-2}]
Cr	Bulk Richardson number criterion for h_{BBL} determination
I_{int}	Vertical integral in Bulk Richardson number criterion
$J(z)$	Weight function $= \vert z\vert/(\vert z\vert + \epsilon h_{BBL})$
V_t	Unresolved shear contribution to the bulk Richardson number
$u_\star$	Surface friction velocity due to wind stress [m.s^{-1}]
u_*^{bot}	Bottom friction velocity due to drag [m.s^{-1}]
δ_E^{bot}	Bottom Ekman depth [m]

Table E1. Variable definitions (cont.).

https://doi.org/10.5194/egusphere-2026-2942
Preprint. Discussion started: 17 July 2026

Symbol	Description
Wave related variables	
$\mathbf{u}^{\mathrm{St}}, w^{St}$	3D Stokes drift [m.s^{-1}]
$\mathbf{u}_p^{\mathrm{St}}$	3D Long-wave Stokes drift [m.s^{-1}]
$\mathbf{u}_e^{\mathrm{St}}$	3D Short-wave Stokes drift [m.s^{-1}]
$\mathbf{U}^{\mathrm{St}}$	2D Stokes transport [m^2.s^{-1}]
$\mathbf{J}$	Horizontal vortex force [m.s^{-2}]
K	Vertical vortex force [m.s^{-2}]
$\mathscr{K}$	Bernoulli head [m^2.s^{-2}]
$\hat{\eta}$	Wave set-down [m]
η^c	Composite sea level [m]
ϕ^c	Composite potential function [s^{-2}]
$\mathscr{P}$	Wave pressure correction [m^2.s^{-2}]
$\mathbf{F}^{\mathbf{w}}$	Non-conservative wave forces [m.s^{-2}]
$\mathbf{A}^{\mathbf{w}}$ or $\mathbf{B}$	Non-conservative wave accelerations [m.s^{-2}]
$\mathbf{B}^{\mathbf{wb}}$	Non-conservative wave force due to wave breaking [m.s^{-2}]
$\mathbf{B}^{\mathbf{str}}$	Non-conservative wave force due to streaming [m.s^{-2}]
$\mathbf{D}^{\mathbf{w}}$	Wave-induced vertical mixing [m.s^{-2}]
K_v^w	Wave-enhanced turbulent eddy viscosity [m^2.s^{-1}]
K_v^{wb}	Turbulent eddy viscosity from wave breaking [m^2.s^{-1}]
ε	Wave dissipation rate [m^3.s^{-3}]
ε^{wb}	Wave dissipation rate due to wave breaking [m^3.s^{-3}]
ε^{str}	Wave dissipation rate due to wave streaming [m^3.s^{-3}]
τ_w	Bottom drag stress due to waves [m^2.s^{-2}]
τ^{wb}	Wave breaking stress [m^2.s^{-2}]
τ^{str}	Bottom streaming stress [m^2.s^{-2}]
$u_\star^{\mathrm{wstr}}$	Friction velocity due to wave streaming [m.s^{-1}]
$\mathbf{u}_{\mathrm{orb}}^w$	Wave orbital velocity [m.s^{-1}]
a_{orb}^w	Semi-orbital excursion [m]
δ_w	Wave bottom boundary layer thickness [m]

Table F1. Variable definitions (cont.).

https://doi.org/10.5194/egusphere-2026-2942
Preprint. Discussion started: 17 July 2026

Wave related variables (cont.)	
k_ξ	ξ-component of wavenumber vector (WKB specific) [rad.m^{-1}]
k_η	η-component of wavenumber vector (WKB specific) [rad.m^{-1}]
E	Depth-integrated wave energy (WKB specific) [kg/s^2]
E^r	Depth-integrated wave roller energy (WKB specific) [kg/s^2]
$\mathscr{A}$	Specific wave action $= E/(\rho_0\sigma)$ (WKB specific) [m^3.s^{-1}]
$\mathscr{A}^r$	Specific roller action $= E^r/(\rho_0\sigma)$ (WKB specific) [m^3.s^{-1}]
c	Phase speed [m.s^{-1}]
$\mathbf{c}_g$	Group velocity vector [m.s^{-1}]
c_0	Depth-refraction coefficient [m^{-1}.s^{-1}]
f_w	Wave friction factor
$\mathscr{H}$	$= kD$
$\mathscr{H}_p$	$= k_pD$
$\mathscr{Z}$	$= k(z+h)$
$\mathscr{V}$	$= \mathbf{k}\cdot\mathbf{u}$
$\mathcal{H}$	Smoothing function Eq. (20)
G	$= g/2\sigma \tanh \mathscr{H}_p / \sinh 2\mathscr{H}_p$
M	Smoothing function Eq. (22)
$\mathcal{T}$	Smoothing function
z_{0s}	Aerobic mixing length scale near the surface [m]
Z	Depth from the surface $= z - \eta - \hat{\eta}$ [m]
z_m	Reference depth above bed [m]
$f(z)$	Vertical shape function with unit integral
$f^b(z)$	Vertical downward decaying shape function with unit integral
$f^{Kv}(z)$	Vertical downward decaying shape function with unit integral
$f^{wd}(z)$	Vertical upward decaying shape function with unit integral
$\ell(z)$	Length scale

Table G1. Variable definitions (cont.).

https://doi.org/10.5194/egusphere-2026-2942
Preprint. Discussion started: 17 July 2026

Wave fields	
$a = a_{\text{wave}}$	Wave amplitude [m]
$H_s = H_\star$	Significant wave height $= 2\sqrt{2}a$ [m]
H_{rms}	RMS wave height $= 2a = \sqrt{8\mathscr{A}\sigma/g}$ [m]
a_f	Filtered wave amplitude [m]
$k = \lvert\mathbf{k}\rvert$	Wavenumber magnitude [rad.m^{-1}]
k_p	Peak wavenumber magnitude [rad.m^{-1}]
T_p	Peak wave period [s]
k_e	Effective wavenumber magnitude [rad.m^{-1}]
σ	Intrinsic radial frequency $= \sqrt{gk\tanh(kD)}$ [rad.s^{-1}]
f	Cyclic frequency $= \sigma/2\pi$ [s^{-1} or Hz]
θ	Wave direction [rad]
$\bar{\theta}$	Spectrally weighted mean wave direction [rad]
θ_p	Peak wave direction [rad]
c_g/k	Group velocity factor [m^2.s^{-1}.rad^{-1}]
c/k	Phase velocity factor [m^2.s^{-1}.rad^{-1}]
A	Wave slope []
μ	Current-to-phase-speed ratio []
WKB Dissipation rates (action units, [m^2.s^{-2}])	
S_b	Breaking dissipation sink $= \varepsilon^{wb}/(\rho_0\sigma)$
S_r	Roller dissipation sink $= \varepsilon^{r}/(\rho_0\sigma)$
S_d	Bottom friction sink $= \varepsilon^{str}/(\rho_0\sigma)$
WKB Parameters (from `wkb_wwave.opt`)	
a_0	Incident wave amplitude [m] ($H_{\text{rms}} = 2a_0$)
θ_0	Incident wave angle [$^\circ$]
T_p	Peak wave period [s]
η_{tide}	Tidal elevation [m]
α_r	Fraction of ε^{wb} feeding roller ($0 \leq \alpha_r \leq 1$)
z_0	Seabed roughness length (Should be the same value as given in the .in for consistency, but the code doesn't enforce that.) [m]
B_b	Breaking intensity coefficient
γ_b	Saturation ratio H_{rms}/D
$\sin\beta$	Roller face slope (≈ 0.1)

Table H1. Variable definitions (cont.).

https://doi.org/10.5194/egusphere-2026-2942
Preprint. Discussion started: 17 July 2026

Environmental/Grid fields	
h	Depth [m]
dx	Horizontal resolution [m]
f	Coriolis acceleration [m.s^{-2}]
D	Total water depth $= h + \eta^c$ (or $h + \eta_{\mathrm{tide}}$ with WKB)
Hardcoded constants	
g	Gravity acceleration [9.81 m.s^{-2}]
κ	Von Kármán constant [0.41]
Ri_c	Critical Richardson number [0.15]
C_{ek}	Ekman depth stabilization constant [258]
ϵ	In Bulk Richardson number criterion [0.1]
Offline parameters	
ρ_0	Reference water density [1027.5 kg.m^{-3}]
ν_h	Horizontal viscosity [0 m^2.s^{-1}]
z_0	Seabed roughness length [m]
H	Tapering depth [30m]
Hardcoded wave parameters	
k_b	Vertical breaking penetration scale $= 1/2ac_b$
c_b	Breaking penetration scale factor $= 0.2$
C_b	Constant controlling wave-breaking-induced vertical mixing magnitude $= 0.03 - 0.1$
k_{Kv}	Vertical breaking scale $= 1/2ac_{Kv}$
c_{Kv}	Constant $= 1.2$
B	Constant $= 4/30$
C	Constant $= -8/3$
D	Constant $= 10/3$
E	Constant $= 0.9508$
k_{wd}	Breaking scale $= 1/c_{wd}\delta_w$
c_{wd}	Constant $= 3$
k_N	Nikuradse roughness $30 \times z_0$ [m]

Table I1. Variable definitions (end).

https://doi.org/10.5194/egusphere-2026-2942
Preprint. Discussion started: 17 July 2026

Author contributions. D.H. led the development of ROMS-NCWEC, including the code merge debugging of the WEC implementation into the current UCLA ROMS codebase, implementing the modified bottom boundary layer thickness criterion accounting for wave streaming, adapting the online momentum diagnostic to WEC, and porting the WKB wave model. D.H. performed the Duck 1994 benchmark validation, designed and ran the L4 Pt. Arguello regional configuration, carried out all analysis, and wrote the manuscript.

D.P.D. contributed initial porting of WEC into the UCLA ROMS codebase, and collaborated with code merge debugging, including increasing the temporal consistency of WEC forces and KPP mixing by recomputing both at the corrector stage of the predictor-corrector time stepping scheme.

M.H. assisted with troubleshooting of ROMS-NCWEC in a realistic regional configuration.

L.R. provided all WaveWatch3 wave forcing files, and implemented the broadband wave approximation and the wave-breaking-induced mixing from Romero et al. (2021) in an earlier version of ROMS-WEC, on which the present implementation builds.

J.C.M. provided scientific guidance throughout, including on the theoretical aspects of wave-current interaction, and contributed to the structure and editing of the manuscript.

All authors contributed to manuscript revisions.

Competing interests. The authors declare that they have no competing interests.

Acknowledgements. This research was supported by the National Science Foundation under grants OCE 2343297, OCE 2124174, OCE 1924686 and OCE 2121646 and by the Office of Naval Research through the allocation N00014-23-1-2812. This work used Expanse supercomputer (Strande et al., 2021) at the San Diego Supercomputer Center from the Advanced Cyberinfrastructure Coordination Ecosystem: Services & Support (ACCESS) program (Boerner et al., 2023), which is supported by U.S. National Science Foundation grants 2138259, 2138286, 2138307, 2137603, and 2138296.

https://doi.org/10.5194/egusphere-2026-2942
Preprint. Discussion started: 17 July 2026

References

Ardhuin, F., Jenkins, A. D., and Belibassakis, K. A.: Comments on "The three-dimensional current and surface wave equations", Journal of Physical Oceanography, 38, 1340–1350, 2008.

Ardhuin, F., Suzuki, N., McWilliams, J. C., and Aiki, H.: Comments on "A combined derivation of the integrated and vertically resolved, coupled wave–current equations", Journal of Physical Oceanography, 47, 2377–2385, 2017.

Battjes, J.: Modeling of turbulence in the surf zone, in: Symp. on Modeling Techniques, pp. 1050–1061, 1975.

Becker, J., Sandwell, D., Smith, W., Braud, J., Binder, B., Depner, J., Fabre, D., Factor, J., Ingalls, S., Kim, S., et al.: Global bathymetry and elevation data at 30 arc seconds resolution: SRTM30_PLUS, Marine Geodesy, 32, 355–371, 2009.

Boerner, T. J., Deems, S., Furlani, T. R., Knuth, S. L., and Towns, J.: Access: Advancing innovation: Nsf's advanced cyberinfrastructure coordination ecosystem: Services & support, in: Practice and Experience in Advanced Research Computing, pp. 173–176, 2023.

Booij, N., Ris, R. C., and Holthuijsen, L. H.: A third-generation wave model for coastal regions: 1. Model description and validation, Journal of geophysical research: Oceans, 104, 7649–7666, 1999.

Breivik, Ø. and Christensen, K. H.: A Combined Stokes Drift Profile under Swell and Wind Sea, Journal of Physical Oceanography, 50, 2819–2833, https://doi.org/10.1175/JPO-D-20-0087.1, 2020.

Breivik, Ø., Janssen, P. A. E. M., and Bidlot, J.-R.: Approximate Stokes Drift Profiles in Deep Water, Journal of Physical Oceanography, 44, 2433–2445, https://doi.org/10.1175/JPO-D-14-0020.1, 2014.

Chen, Z., Wenegrat, J., Chor, T., and Marchesiello, P.: Evaluating turbulence parameterizations at gray zone resolutions for the ocean surface boundary layer, Journal of Advances in Modeling Earth Systems, 17, e2025MS005 104, 2025.

Church, J. C. and Thornton, E. B.: Effects of breaking wave induced turbulence within a longshore current model, Coastal engineering, 20, 1–28, 1993.

Couvelard, X., Lemarié, F., Samson, G., Redelsperger, J.-L., Ardhuin, F., Benshila, R., and Madec, G.: Development of a two-way-coupled ocean–wave model: assessment on a global NEMO (v3. 6)–WW3 (v6. 02) coupled configuration, Geoscientific Model Development, 13, 3067–3090, 2020.

Dauhajre, D. P., McWilliams, J. C., and Uchiyama, Y.: Submesoscale coherent structures on the continental shelf, Journal of Physical Oceanography, 47, 2949–2976, 2017.

Dauhajre, D. P., McWilliams, J. C., and Renault, L.: Nearshore Lagrangian connectivity: Submesoscale influence and resolution sensitivity, Journal of Geophysical Research: Oceans, 124, 5180–5204, 2019.

Faria, A. G., Thornton, E., Stanton, T., Soares, C. k., and Lippmann, T.: Vertical profiles of longshore currents and related bed shear stress and bottom roughness, Journal of Geophysical Research: Oceans, 103, 3217–3232, 1998.

Faria, A. G., Thornton, E., Lippmann, T., and Stanton, T.: Undertow over a barred beach, Journal of Geophysical Research: Oceans, 105, 16 999–17 010, 2000.

Feddersen, F. and Trowbridge, J.: The effect of wave breaking on surf-zone turbulence and alongshore currents: A modeling study, Journal of Physical Oceanography, 35, 2187–2203, 2005.

Feddersen, F., Guza, R., Elgar, S., and Herbers, T.: Cross-shore structure of longshore currents during Duck94, in: Coastal Engineering 1996, pp. 3666–3679, 1997.

Feddersen, F., Guza, R. T., Elgar, S., and Herbers, T. H. C.: Velocity Moments in Alongshore Bottom Stress Parameterizations, Journal of Geophysical Research: Oceans, 105, 8673–8686, https://doi.org/10.1029/2000JC900015, 2000.

Gallagher, E. L., Elgar, S., and Guza, R.: Observations of sand bar evolution on a natural beach, Journal of Geophysical Research: Oceans, 103, 3203–3215, 1998.

Hell, M., Fox-Kemper, B., and Chapron, B.: A particle-in-cell wave model for efficient sea-state estimates in Earth system models—PiCLES, Journal of Advances in Modeling Earth Systems, 17, e2025MS005 221, 2025.

Hypolite, D., Romero, L., McWilliams, J. C., and Dauhajre, D. P.: Surface gravity wave effects on submesoscale currents in the open ocean, Journal of Physical Oceanography, 51, 3365–3383, 2021.

Hypolite, D., Romero, L., McWilliams, J. C., and Dauhajre, D. P.: Langmuir circulations transfer kinetic energy from submesoscales and larger scales to dissipative scales, Journal of Physical Oceanography, 53, 253–268, 2023.

Hypolite, D., Dauhajre, D. P., Ho, M., Romero, L., and McWilliams, J. C.: UCLA-ROMS-NCWEC: The Regional Oceanic Modeling System with Non-Conservative Surface Gravity Wave Effects on Currents, https://doi.org/10.5281/zenodo.20498888, 2026a.

Hypolite, D., Dauhajre, D. P., Ho, M., Romero, L., and McWilliams, J. C.: ROMS-NCWEC Pt. Arguello configuration: grid, initial and boundary conditions, WaveWatch3 forcing and representative model output, https://doi.org/10.5281/zenodo.20499100, 2026b.

Hypolite, D., Dauhajre, D. P., Ho, M., Romero, L., and McWilliams, J. C.: ROMS-NCWEC Duck 1994 Configuration: Grid, Wave Forcing, Input File, and Override Source Code, https://doi.org/10.5281/zenodo.21384107, 2026c.

Jackett, D. R. and Mcdougall, T. J.: Minimal adjustment of hydrographic profiles to achieve static stability, Journal of Atmospheric and Oceanic Technology, 12, 381–389, 1995.

Kirby, J. T., Wei, G., Chen, Q., Kennedy, A. B., and Dalrymple, R. A.: FUNWAVE 1.0: fully nonlinear Boussinesq wave model-Documentation and user's manual, Tech. rep., University of Delaware, 1998.

Klopman, G.: Stokes Transport, Technical Report H840.30, Part II, WL-Delft Hydraulics, 1994.

Kumar, N., Voulgaris, G., Warner, J. C., and Olabarrieta, M.: Implementation of the Vortex Force Formalism in the Coupled Ocean-Atmosphere-Wave-Sediment Transport (COAWST) Modeling System for Inner Shelf and Surf Zone Applications, Ocean Modelling, 47, 65–95, https://doi.org/10.1016/j.ocemod.2012.01.003, 2012.

Kumar, N., Cahl, D. L., Crosby, S. C., and Voulgaris, G.: Bulk versus spectral wave parameters: Implications on stokes drift estimates, regional wave modeling, and HF radars applications, Journal of Physical Oceanography, 47, 1413–1431, 2017.

Lane, E. M., Restrepo, J., and McWilliams, J. C.: Wave–current interaction: A comparison of radiation-stress and vortex-force representations, Journal of physical oceanography, 37, 1122–1141, 2007.

Large, W. G., McWilliams, J. C., and Doney, S. C.: Oceanic Vertical Mixing: A Review and a Model with a Nonlocal Boundary Layer Parameterization, Reviews of Geophysics, 32, 363–403, https://doi.org/10.1029/94RG01872, 1994.

Lentz, S., Guza, R., Elgar, S., Feddersen, F., and Herbers, T.: Momentum balances on the North Carolina inner shelf, Journal of Geophysical Research: Oceans, 104, 18 205–18 226, 1999.

Lentz, S. J. and Fewings, M. R.: The wind-and wave-driven inner-shelf circulation, Annual review of marine science, 4, 317–343, 2012.

Madsen, O. S.: Spectral wave-current bottom boundary layer flows, in: Coastal engineering 1994, pp. 384–398, 1994.

Marchesiello, P., Auclair, F., Debreu, L., McWilliams, J., Almar, R., Benshila, R., and Dumas, F.: Tridimensional nonhydrostatic transient rip currents in a wave-resolving model, Ocean Modelling, 163, 101 816, 2021.

McWilliams, J.: Surface wave dissipation and current acceleration, J. Fluid Mech., submitted, 2026.

McWilliams, J. C.: Submesoscale currents in the ocean, Proceedings of the Royal Society A: Mathematical, Physical and Engineering Sciences, 472, 2016.

https://doi.org/10.5194/egusphere-2026-2942
Preprint. Discussion started: 17 July 2026

McWilliams, J. C., Restrepo, J. M., and Lane, E. M.: An Asymptotic Theory for the Interaction of Waves and Currents in Coastal Waters, Journal of Fluid Mechanics, 511, 135–178, https://doi.org/10.1017/S0022112004009358, 2004.

Moghimi, S., Thomson, J., Özkan-Haller, T., Umlauf, L., and Zippel, S.: On the modeling of wave-enhanced turbulence nearshore, Ocean Modelling, 103, 118–132, 2016.

Newberger, P. and Allen, J. S.: Forcing a three-dimensional, hydrostatic, primitive-equation model for application in the surf zone: 2. Application to DUCK94, Journal of Geophysical Research: Oceans, 112, 2007.

Renault, L., Molemaker, M. J., McWilliams, J. C., Shchepetkin, A. F., Lemarié, F., Chelton, D., Illig, S., and Hall, A.: Modulation of Wind Work by Oceanic Current Interaction with the Atmosphere, Journal of Physical Oceanography, 46, 1685–1704, https://doi.org/10.1175/JPO-D-15-0232.1, 2016.

Reniers, A., Thornton, E., Stanton, T., and Roelvink, J.: Vertical flow structure during Sandy Duck: observations and modeling, Coastal Engineering, 51, 237–260, 2004.

Romero, L., Hypolite, D., and McWilliams, J. C.: Submesoscale current effects on surface waves, Ocean Modelling, 153, 101 662, 2020.

Romero, L., Hypolite, D., and McWilliams, J. C.: Representing Wave Effects on Currents, Ocean Modelling, 167, 101 873, https://doi.org/10.1016/j.ocemod.2021.101873, 2021.

Roullet, G., Molemaker, M. J., Ducousso, N., and Dubos, T.: Compact Symmetric Poisson Equation Discretization for Non-Hydrostatic Sigma Coordinates Ocean Model, Ocean Modelling, 118, 107–117, https://doi.org/10.1016/j.ocemod.2017.09.001, 2017.

Shchepetkin, A. F. and McWilliams, J. C.: A Method for Computing Horizontal Pressure-Gradient Force in an Oceanic Model with a Nonaligned Vertical Coordinate, Journal of Geophysical Research: Oceans, 108, 3090, https://doi.org/10.1029/2001JC001047, 2003.

Shchepetkin, A. F. and McWilliams, J. C.: The Regional Oceanic Modeling System (ROMS): A Split-Explicit, Free-Surface, Topography-Following-Coordinate Oceanic Model, Ocean Modelling, 9, 347–404, https://doi.org/10.1016/j.ocemod.2004.08.002, 2005.

Shi, F., Kirby, J. T., and Tehranirad, B.: Tsunami benchmark results for spherical coordinate version of FUNWAVE-TVD, Center for Applied Coastal Research, University of Delaware, Tech. Rep. CACR-12-02, 2012.

Soulsby, R. L.: Bed Shear-Stresses Due to Combined Waves and Currents, in: Advances in Coastal Morphodynamics, edited by Stive, M. J. F., de Vriend, H. J., Fredsoe, J., Hamm, L., Soulsby, R. L., Teisson, C., and Winterwerp, J. C., pp. 4–20–4–23, Delft Hydraulics, Delft, Netherlands, 1995.

Soulsby, R. L., Hamm, L., Klopman, G., Myrhaug, D., Simons, R. R., and Thomas, G. P.: Wave-current interaction within and outside the bottom boundary layer, Coastal engineering, 21, 41–69, 1993.

Strande, S., Cai, H., Tatineni, M., Pfeiffer, W., Irving, C., Majumdar, A., Mishin, D., Sinkovits, R., Norman, M., Wolter, N., et al.: Expanse: computing without boundaries: architecture, deployment, and early operations experiences of a supercomputer designed for the rapid evolution in science and engineering, in: Practice and Experience in Advanced Research Computing, pp. 1–4, 2021.

Sutherland, P. and Melville, W. K.: Field measurements of surface and near-surface turbulence in the presence of breaking waves, Journal of Physical Oceanography, 45, 943–965, 2015.

Terray, E., Drennan, W., and Donelan, M.: The vertical structure of shear and dissipation in the ocean surface layer, https://apps.dtic.mil/sti/html/tr/ADA365369/, 1999.

Thornton, E. B. and Guza, R.: Transformation of wave height distribution, Journal of Geophysical Research: Oceans, 88, 5925–5938, 1983.

Tolman, H. L.: User Manual and System Documentation of WAVEWATCH III Version 3.14, Technical Note 276, NOAA/NWS/NCEP/MMAB, 2009.

https://doi.org/10.5194/egusphere-2026-2942
Preprint. Discussion started: 17 July 2026

Treillou, S., Marchesiello, P., Baker, C. M., McWilliams, J., and Dumas, F.: Tracer dispersion by surfzone eddies: assessing the impact of undertow vertical shear, Journal of Physical Oceanography, 55, 1211–1234, 2025.

Uchiyama, Y., McWilliams, J. C., and Shchepetkin, A. F.: Wave–Current Interaction in an Oceanic Circulation Model with a Vortex-Force Formalism: Application to the Surf Zone, Ocean Modelling, 34, 16–35, https://doi.org/10.1016/j.ocemod.2010.04.002, 2010.

Wang, P., McWilliams, J. C., Uchiyama, Y., Chekroun, M. D., and Yi, D. L.: Effects of wave streaming and wave variations on nearshore wave-driven circulation, Journal of Physical Oceanography, 50, 3025–3041, 2020.

Warner, J. C., Armstrong, B., He, R., and Zambon, J. B.: Development of a coupled ocean–atmosphere–wave–sediment transport (COAWST) modeling system, Ocean modelling, 35, 230–244, 2010.

Wu, X., Feddersen, F., and Giddings, S. N.: Diagnosing surfzone impacts on inner-shelf flow spatial variability using realistic model experiments with and without surface gravity waves, Journal of Physical Oceanography, 51, 2505–2515, 2021.

Wyngaard, J. C.: Toward numerical modeling in the "Terra Incognita", Journal of the atmospheric sciences, 61, 1816–1826, 2004.

Zijlema, M., Stelling, G., and Smit, P.: SWASH: An operational public domain code for simulating wave fields and rapidly varied flows in coastal waters, Coastal Engineering, 58, 992–1012, 2011.